J Mammal Evol (2015) 22:141–167
DOI 10.1007/s10914-014-9271-8

ORIGINAL PAPER

Sexually Dimorphic Bandicoots (Marsupialia: Peramelemorphia) From the Oligo-Miocene of Australia, First Cranial Ontogeny for Fossil Bandicoots and New Species Descriptions

Kenny J. Travouillon · Michael Archer · Suzanne J. Hand · Jeanette Muirhead

Published online: 4 September 2014

Abstract Peramelemorphians (bandicoots and bilbies) are unique among mammals in having the shortest gestation period. Very little is known about their evolutionary history primarily because until recently their fossil record was scarce. Here we describe two new species, *Madju variae,* gen. et sp. nov., from late Oligocene to middle Miocene deposits from the Riversleigh World Heritage Area, Queensland, and the Kutjamarpu Local Fauna, South Australia, and *Madju encorensis,* gen. et sp. nov., also from Riversleigh WHA but from the late middle to early late Miocene. Phylogenetic analysis suggests that they are best regarded as basal members of the Superfamily Perameloidea. Species of *Madju* are unusual in showing a distinct reduction in size through time, possibly reflecting environmental change from the early to late Miocene. *Madju variae* is the first-known sexually dimorphic fossil peramelemorphian. The preservation and representation of specimens of *M. variae* is exceptional, enabling documentation of ontogenetic development from juvenile to old adult stage suggesting that juveniles of *M. variae* developed more slowly than their modern counterparts and that lactation lasted for a longer time. If so, the short gestation of modern peramelemorphians would appear to be a specialisation that might have evolved sometime after the middle Miocene.

Keywords Fossil bandicoots · Sexual dimorphism · Cranial ontogeny · Riversleigh World Heritage Area · Kutjamarpu Local Fauna

Introduction

Recent advances in our understanding of the evolution of peramelemorphians (bandicoots and bilbies), an order of marsupials from Sahul (Australia, New Guinea and neighbouring islands), has been principally due to molecular systematics (e.g., Westerman et al. 1999, 2001, 2012; Westerman and Krajewski 2000; Meredith et al. 2008) and the discovery of near-complete fossil specimens from the Riversleigh World Heritage Area (WHA) of northwestern Queensland (Muirhead 2000; Travouillon et al. 2010, 2013a; Gurovich et al. 2013). This order contains four families: Chaeropodidae, which contains the recently extinct Pig-footed Bandicoot (*Chaeropus ecaudatus*); Thylacomyidae, containing four species of bilby (two species of *Macrotis*, the fossil species *Ischnodon australis* from Pliocene deposits of central Australia, and the middle Miocene *Liyamayi dayi*); Peramelidae, subdivided into three subfamilies, Peramelinae (mostly living species in the genera *Perameles* and *Isoodon* and the Miocene *Crash bandicoot*), Echymiperinae (containing mostly living New Guinean taxa in the genera *Echymipera, Microperoryctes,* and *Rhynchomeles*), and Peroryctinae (containing the living New Guinean genus *Peroryctes*); and Yaralidae, a family of small insectivorous Miocene bandicoots in the genus *Yarala*. Species of *Galadi* from Miocene deposits of Riversleigh WHA (Travouillon et al. 2010, 2013a), *Bulungu* from Oligocene and Miocene deposits from the Etadunna Formation (South Australia) and Riversleigh WHA (Gurovich et al. 2013; Travouillon et al. 2013b), and cf. *Peroryctes* from Pliocene Hamilton Local Fauna (LF), Victoria (Turnbull et al. 2003) appear to represent basal

Electronic supplementary material The online version of this article (doi:10.1007/s10914-014-9271-8) contains supplementary material, which is available to authorized users.

K. J. Travouillon (✉) · J. Muirhead
School of Earth Sciences, University of Queensland, St Lucia, Queensland 4072, Australia
e-mail: kennytravouillon@hotmail.com

K. J. Travouillon · M. Archer · S. J. Hand
School of Biological, Earth and Environmental Sciences, University of New South Wales, Sydney, New South Wales 2052, Australia

peramelemorphians that are closer to crown group Peramelemorphia (Peramelidae + Thylacomyidae + Chaeropodidae) than Yaralidae (Gurovich et al. 2013; Travouillon et al. 2013a,b).

The peramelemorphian fossil record has until recently been restricted mostly to teeth, maxillae, and dentaries. However, fossils from the Riversleigh WHA have included near complete skulls such as those known for *Yarala burchfieldi* (Muirhead 2000), *Galadi speciosus* (Travouillon et al. 2010), *G. amplus* (Travouillon et al. 2013a), and *Bulungu palara* (Gurovich et al. 2013). Of these, only *G. speciosus* is represented by more than one skull.

Here, we describe two new peramelemorphians from the Oligo-Miocene deposits of the Riversleigh WHA and the Kutjamarpu LF, Wipajiri Formation, South Australia. The first of these two is represented by 11 partial skulls, five of which are complete enough to show the first evidence of sexual dimorphism in fossil peramelemorphians and cranial ontogeny for arguably ancestral members of this group.

Materials and Methods

Specimens described here were collected from the Riversleigh World Heritage Area, northwestern Queensland over the past 38 years by teams led by the University of New South Wales researchers. A combined South Australian Museum and University of California expedition in 1971 collected specimens from the Leaf Locality, Kutjamarpu Local Fauna (LF). Riversleigh WHA specimens were recovered by acid-processing of limestone blocks while Leaf Locality specimens were screen washed in the field. All specimens are registered with the Queensland Museum Fossil Collection (prefix **QM F**), Brisbane, Australia, except for one specimen from the Leaf Locality, which is registered with the University of California, Museum of Paleontology (prefix **UCMP**), USA.

Terminology

Higher-level marsupial systematics follows Aplin and Archer (1987). Peramelemorphian systematics follows Muirhead (1994, 2000), Muirhead and Filan (1995), Travouillon et al. (2010), and Westerman et al. (2012). Cranial and dental terminology follows Archer (1976), Muirhead (1994, 2000), Muirhead and Filan (1995), Turnbull et al. (2003), Voss and Jansa (2003), Wible (2003), Beck (2008), and Travouillon et al. (2010). Molar and dP3 loci homology follows Luckett (1993). Riversleigh WHA nomenclature follows Arena (2004), and Travouillon et al. (2006, 2011).

Qualitative and Quantitative Analyses

The absolute age of individuals of *Madju variae,* gen. et sp. nov., could not be determined (following Black et al. 2010) and for this reason, an arbitrary system was developed for defining the relative age of each individual. The age stages are shown in Table 1, for upper and lower jaws (some of which are associated), with corresponding specimen numbers, defined by tooth eruption, wear, and elevation of premolars. Due to the nature of the fossil material, we were unable to quantitatively assess allometric growth using the methods of Black et al. (2010) or Flores et al. (2013). Instead, a qualitative comparison of specimens from each stage of development was added in the result section.

We performed dental morphometric analyses to determine changes in variation over time in the dental morphology of the two species of *Madju,* gen. nov., described here. This was done by separating specimens belonging in different Riversleigh Faunal Zones (B= early Miocene; C = middle Miocene; D = early late Miocene). Specimens from Faunal Zone A (late Oligocene) were not included due to low sample size. We measured and plotted length versus width of each upper and lower premolar and molar (see Appendices 1–4 for complete list of specimen and measurements). We have also identified probable males and females on the basis of the size of upper and lower canines and the robusticity of the zygomatic arches. In the majority of modern peramelemorphian species, including species of *Isoodon, Perameles, Macrotis, Echymipera,* and *Peroryctes,* males and females are dimorphic. Males are considerably bigger, with markedly enlarged upper and lower canines (Strahan 1995; Flores et al. 2013). Males identified on this basis within the fossil samples include: QM F23430, F39857, F23406, F20890, F23431, F29705, F57323, F57361, F23724, and F57411. Females identified include: QM F57433, F23405, F57359, F23800, F57384, F57380, F39853, F24420, F57367, F57362, F24419, F57400, F57407, F57412, F57413, and F57427. All males and females so determined are from Riversleigh's Faunal Zone B.

We also calculated univariate statistics and coefficients of variation for all samples referred to *Madju variae*, gen. et sp. nov., but we were not able to do so for *Madju encorensis*, sp. nov., due to small sample size (see Appendix 5).

Phylogenetic Analysis

We analyzed the phylogenetic relationship of species of *Madju*, gen. nov., using the matrix from Travouillon et al.

Table 1 Stages of development of *Madju variae,* showing teeth eruption, tooth wear, and premolar elevation

Upper Jaw													
Specimen number	Stage	I1-4/5?	C	P1	P2	dP3	P3	M1	M2	M3	M4	Tooth wear	Premolar elevation
QM F36336	Stage I	+*	+*	+*	+*	+*	0	+	+*	0*	0*	None	Not known
QM F57321	Stage II	+*	+	+*	+*	+*	0	+	+	+*	0*	None	Not known
QM F57978	Stage IIIa	+*	+	+	+	+	0	+	+	+	−	None	Not elevated
QM F23405	Stage IV	+*	+	+*	+*	shed*	+*	+	+	+	+*	Light wear	Not known
QM F23430	Stage V	+*	+	+*	+*	shed	+	+	+*	+*	+*	Medium wear on all teeth	Elevated
QM F23406	Stage VI	+*	+*	+*	+*	shed*	+*	+	+	+	+	Heavy wear on all teeth	Not known
Lower Jaw													
Specimen number	Stage	i1-3	c	p1	p2	dp3	p3	m1	m2	m3	m4	Tooth wear	Premolar elevation
QM F24328	Stage I	+*	+*	+*	+	+*	0	+	+	−*	0	None	Not elevated
QM F57321	Stage II	+*	+*	+*	+	+*	0	+	+	+	−	None	Not elevated
QM F57978	Stage IIIa	+*	+	+	+	+	0	+	+	+*	−	None	Not elevated
QM F57379	Stage IIIb	+	+	+	+	+	0	+	+	+	+	None	Not elevated
QM F57437	Stage IIIc	+	+	+	+	shed	−	+	+	+	+	Wear on m1 only	Not elevated
QM F24227	Stage IV	+*	+*	+	+	shed	+	+	+	+	+	Light wear p1-2, m1-3	p1 and p2 elevated
QM F57323	Stage V	+*	+	+	+	shed	+	+*	+	+*	+	Medium wear on all teeth	Elevated and p3 reclined
QM F23431	Stage VI	+*	+	+	+	shed*	+*	+	+	+	+	Heavy wear on all teeth	Elevated and p1-3 reclined

+, fully erupted; −, erupting; 0, not visible at all; I/i, incisor; C/c, canine; dP/dp/, deciduous premolar; P/p, premolar; M/m, molar. Inferred presence of teeth, either by well-developed alveoli or from presence in previous stage, are marks with an asterisk

(2013b). The matrix (see Appendix 6) comprises 156 qualitative morphological characters (123 dental and 33 cranial). Seventy-one characters were ordered in all analyses. We scored and added to the matrix both species of *Madju*, gen. nov., described below, resulting in the analysis of 46 taxa. Following Travouillon et al. (2013b), we used *Djarthia murgonensis, Barinya wangala, Mutpuracinus archibaldi, Dasyurus hallucatus, Dasyuroides byrnei, Phascogale tapoatafa, Antechinus stuartii*, and *Sminthopsis macroura* as outgroups.

Parsimony Analysis

Two parsimony analyses of the matrix, one unconstrained, the other constrained, were performed using PAUP* 4.0b10 (Swofford 2002). For the unconstrained maximum parsimony analysis, a two-stage search strategy was implemented, with an initial search comprising 1,000 heuristic replicates, saving ten trees per replicate, followed by a second heuristic search within the trees saved from the first stage, following Worthy et al. (2006) and Beck et al. (2008). The multiple most parsimonious trees were summarized using strict consensus with bootstrap values calculated using 1000 bootstrap replicates comprised of ten random addition sequence replicates each. Decay indices were also calculated using TreeRot 3.0 (Sorenson and Franzosa 2007).

Following Travouillon et al. (2013b), the constrained parsimony analysis was analyzed using the same methods as the unconstrained maximum parsimony analysis, with a 'molecular scaffold' implemented as a 'backbone' constraint, using the molecular phylogeny of Westerman et al. (2012).

Bayesian Analysis

Two Bayesian analyses of the matrix, one unconstrained and one constrained, were implemented with MrBayes 3.2 using Lewis (2001)'s 'Mk' model for discrete morphological characters. The unconstrained analysis was run for 20 million generations, with a sampling frequency of 2000. The potential scale reduction factor (PSRF) and minimum and average effective sample sizes (ESS) for both the tree length and alpha parameters were 1.0 and >5000, respectively, indicating that stationarity and convergence had been achieved for post-burn-in trees. The post-burn-in trees were summarized using 50 % majority rule consensus, with Bayesian posterior probabilities as support values. This method was repeated with the 'molecular scaffold' implemented using multiple 'partial' constraints, with each constraint corresponding to a node in the molecular scaffold.

Systematic Paleontology

Order PERAMELEMORPHIA (Kirsch, 1968) Aplin and Archer, 1987

Superfamily Perameloidea (Waterhouse, 1838)
Family incertae sedis
Madju, gen. nov.

Type Species *Madju variae*, sp. nov.

Generic Diagnosis Species of *Madju* differ from species of *Chaeropus* (Chaeropodidae) in having an anterior cingulum on all upper molars, a weakly developed metaconular hypocone, preparacrista connected to stylar cusp B on M1, no anterior cuspid on p1, and cristid obliqua terminates lingual to protocone on m1-3. They differ from species of *Macrotis*, *Ischnodon,* and *Liyamayi* (Thylacomyidae) in having a well-developed paraconid on m1, an oval entoconid with anteriorly directed preentocristid on m1-4, and more triangular upper molars. They differ from species of *Perameles, Crash,* and *Isoodon* (Peramelinae) in having weakly developed metaconular hypocone, posterior cingulum absent on all upper molars, stylar cusp B on M2 is oval, crested, and connects to preparacrista, entoconid is oval with anteriorly directed preentocristid on m1-4, and stylar cusp C present on M1 and M3. They differ from *Peroryctes* (Peroryctinae) in lacking enlarged upper and lower third premolars, and hypoflexid present on m1. They differ from species of *Echymipera, Microperoryctes,* and *Rhynchomeles* (Echypimerinae) in having a hypoflexid on m1 and a paraconid-metaconid distance is shorter than metaconid-protoconid distance on m4. They differ from Oligo-Miocene species of *Yarala*, *Galadi,* and *Bulungu* in having the postparacrista and premetacrista not connected to form a centrocrista on M1-3, squamosal-frontal contact each other, posterior ends of the nasals terminating anterior to the orbital fossa, and having a secondary foramen ovale present.

Generic Etymology "Madju," after a Waanyi Aboriginal word from the Riversleigh district meaning 'sister' (G. Breen pers. comm., J. M.), in reference to the apparent similarity of this genus to all Recent bandicoot taxa and the probable sister-group relationship. The gender of this genus is considered to be feminine.

Madju variae, sp. nov. (Figs. 1, 2, 3, 4, 5, 6, and 7)

Holotype QM F57978, partial juvenile skull with left P1, M1-3, M4 in crypt, right P1-2, M1-3, M4 in crypt, associated dentaries with left p1-2, m1-4, right p2, m1-4 (m2 and m4 are damaged), and associated vertebrae and postcranials.

Paratypes QM F23405, partial sub-adult skull with left M1-2, broken M3, right broken C, M1-2, associated dentaries with left p1-m4, right i3 and p1; F23406, left side of skull with M1-4; F23429, left maxilla with M1-4; F23430, left maxilla with C, P1-3, M1 and M3; F23431, left dentary with c, p1-3, m1-4; F24227, right dentary with p1-3, m1-4; F24328, juvenile left dentary with p2, m1-2; F36336, partial juvenile skull with right M1; F57321, partial juvenile skull with left M1-2, associated dentaries with left p2, m1-3, right m1-2; F57322, right maxilla with M1-4; F57323, associated dentaries with right c, p1-3, m2-3, left c, p1-3, m2, m4; F57324, partial juvenile skull with left P1-2, M1, M4, right m1-3, associated dentaries with left p2, m1, m3-4, right p1-2, m1, m3, and postcranials; F57379, associated dentaries with right c, p1-2, dp3, m1-4, left p2, dp3, m1-3; F57437, juvenile left maxilla with broken m2, m3-4, and associated dentaries with left c, p1-2, p3 unerupted, m1-4, right i2-3, c, p1-2, p3 unerupted, m1-4.

Fig. 1 *Madju variae,* gen. et sp. nov., juvenile skull with dentary, holotype QM F57978, stage IIIa of ontogenetic series. **a**, dorsal view of skull; **b**, ventral view of the skull; **c**, right lateral view of skull; **d**, left lateral view of skull and left dentary in lateral view. **Abbreviations**: **amp**, accessory palatal fenestrae; **ang**, angular process; **aofo**, antorbital fossa; **as**, alisphenoid; **astp**, alisphenoid tympanic process; **bs**, basisphenoid; **C**, upper canine; **c**, lower canine; **cf**, carotid foramen, **con**, mandibular condyle; **cor**, coronoid process; **dP3**, deciduous third upper premolar; **dp3**, deciduous third lower premolar; **eam**, external auditory meatus; **fgpn**, foramen for greater petrosal nerve; **fm**, foramen magnum; **fr**, frontal; **fro**, foramen rotundum; **gf**, glenoid fossa; **gpas**, glenoid process of alisphenoid; **in**, internal nares; **iof**, infraorbital foramen; **ips**, foramen for inferior petrosal sinus; **ju**, jugal; **lac**, lacrimal; **lacf**, lacrimal formamen; **ls**, lambdoidal sesamoid; **M1-M4**, upper molar one to four; **m1-m4**, lower molar one tofour; **ma**, mastoid; **maf**, masseteric fossa; **mf**, mental foramen; **mp**, maxillopalatine fenestrae; **mx**, maxilla; **na**, nasal; **P1-P3**, upper premolar one to three; **p1-p3**, lower premolar one to three; **pa**, parietal; **pal**, palatine; **pe**, petrosal; **pfo**, primary foramen ovale; **pgp**, postglenoid process; **pmx**, premaxilla; **ps**, presphenoid; **pt**, pterygoid; **ptp**, posttympanic process; **sfo**, secondary foramen ovale; **smf**, suprameatal foramen; **so**, supraoccipital; **sof**, sphenorbital fissure; **sq**, squamosal; **tf**, transverse foramen. Scale bar equals 1 cm

Referred Material Additional specimens referred to *Madju variae* have been collected from the following locations - AL90 Site: QM F50891, left dentary with broken p2-p3, m4; Cadbury's Kingdom Site: F57447, right maxilla with M1-2; F57448, left M2; F57449, right dentary with m3-4; Camel Sputum Site: F23291, left dentary with p1-2, m2-4; F24672, right maxilla with P3, M1-4; F29705, left dentary with m1-4; F57355, right maxilla with P1-3, M1-4; F57356, right dentary with m3-4; F57357, right dentary with m1-4; F57358, left maxilla with M3-4; F57359, left maxilla with C, P1, P3, M1-2; F57360, left maxilla with M2-4; F57361, left dentary with c, p1-3; F57362, right dentary with c, p1, p3, m3-4; F57363, left dentary with m4; F57364, left dentary with m4; F57365, left dentary with m2-4; F57366, left maxilla with M1, M3; F57367, right dentary with c, p2-3, m1-4; F57368, right dentary with p3, m3; F57369, right M3; F57370, left dentary with p2-3, m1; F57371, right dentary with p2-3, m1; F57372, left maxilla with M3-4; F57373, left dentary with m1-2; F57374, right dentary with m4; F57375, left dentary with m3-4; F57376, left dentary with m2-3; F57377, right maxilla with M1-4; F57378, left maxilla with M4; Creaser's Ramparts Site: F23724, left dentary with c, p1; F24303, left

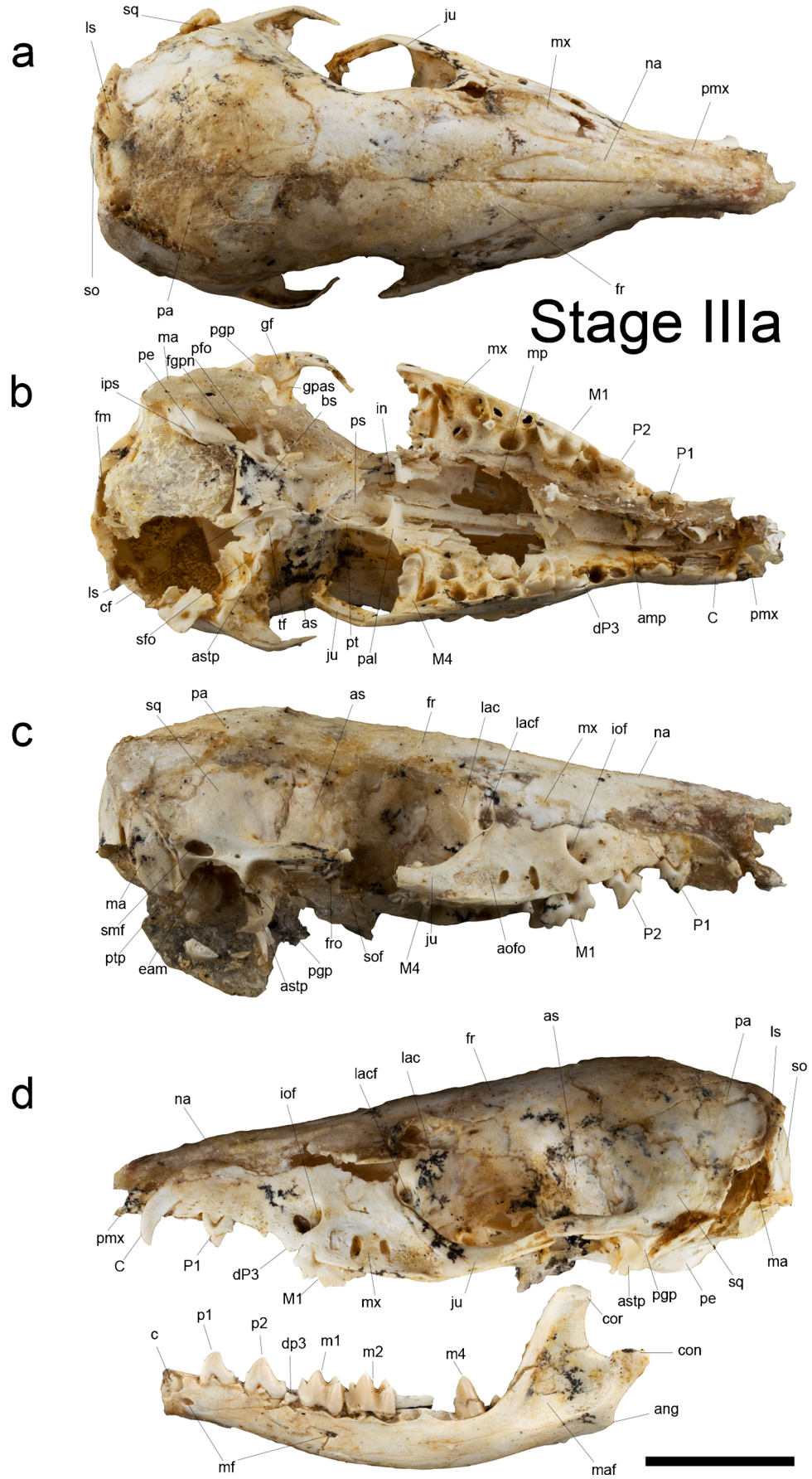
a
sq
ls
ju
mx
na
pmx
so
pa
fr
Stage IIIa
b
pgp
gf
ma
pfo
pe
fgpn
mx
mp
ips
gpas
bs
M1
fm
in
ps
P2
P1
ls
cf
tf
as
sfo
astp
ju
pt
pal
M4
dP3
amp
C
pmx
c
sq
pa
as
fr
lac
lacf
mx
iof
na
ma
smf
ptp
eam
pgp
astp
fro
sof
ju
M4
aofo
M1
P2
P1
d
as
pa
ls
so
fr
lac
lacf
na
iof
pmx
C
P1
dP3
M1
mx
ju
astp
pgp
pe
sq
ma
cor
p1
p2
c
dp3
m1
m2
m4
con
ang
mf
maf

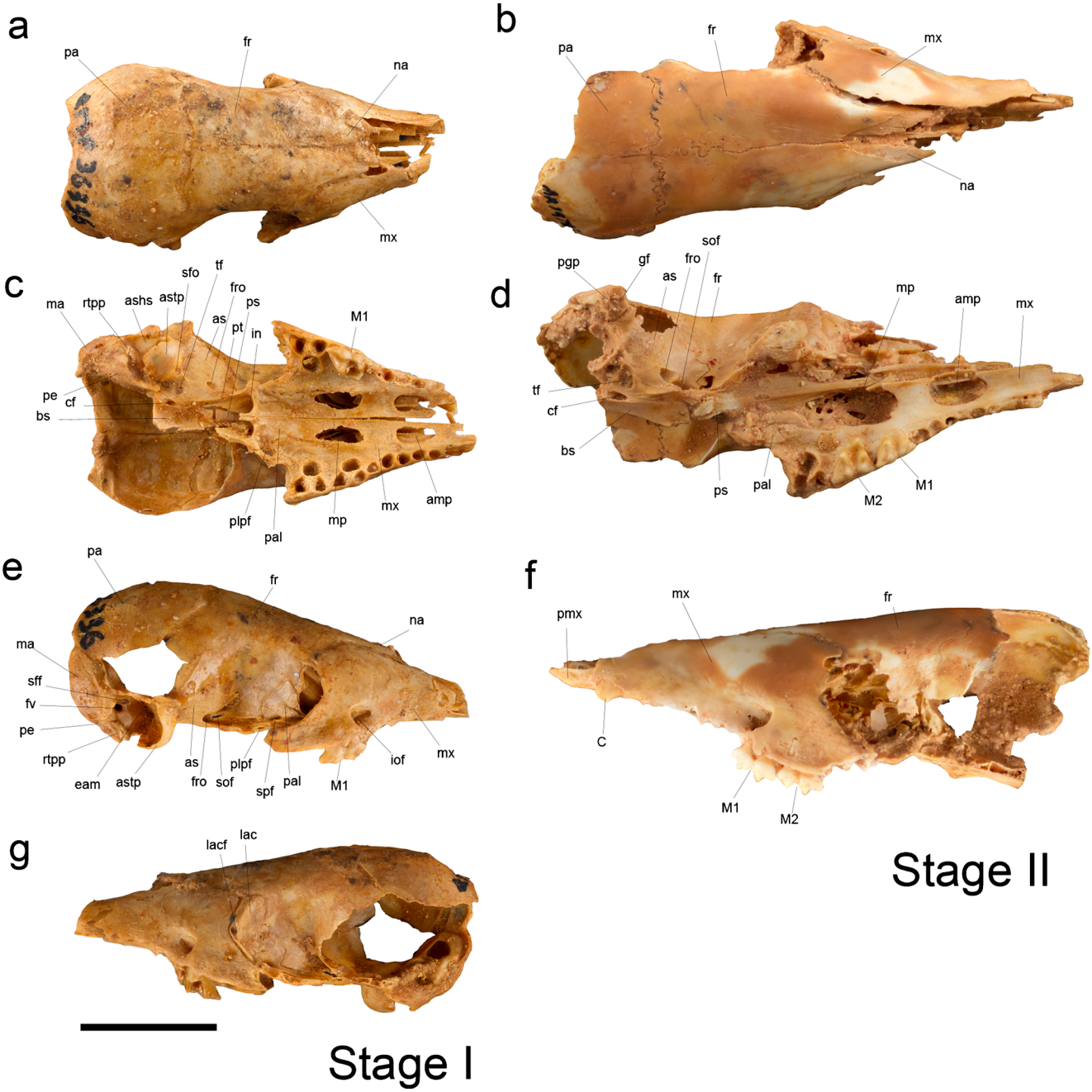

Fig. 2 *Madju variae,* gen. et sp. nov., juvenile skulls, paratype QM F36336 (**a**, **c**, **e,** and **g**), stage I of ontogenetic series and paratype QM F57321 (**b**, **d,** and **f**), stage II of ontogenetic series. **a-b**, dorsal view of skulls; **c-d**, ventral view of skulls; **e**, right lateral view of skull; **f-g**, left lateral view of skulls. **Abbreviations**: **ashs**, alisphenoid hypotympanic sinus; **fv**, fenestra vestibuli; **plpf**, posterolateral palatal foramen; **rtpp**, rostral tympanic process of petrosal; **sff**, secondary facial foramen; **spf**, sphenopalatine foramen. For all other abbreviations, refer to Fig. 1. Scale bar equals 1 cm

dentary p3, m3-4; Dirk's Towers Site: F20890, left dentary p2, m3-4; F39857, partial crushed skull with left P1, right P2, M1-4; F57450, right maxilla with m2-4 ; Gag Site: F57440, right maxilla with m3-4; F57441, left dentary with p1-2, m1; F57442, right dentary with m4; F57443, right dentary with m1-4; F57444, right dentary with m2, m4; F57445, right maxilla with m3-4; Golden Steph Site: F57469, right dentary with p3, m1-3; Gotham City Site: F57465, left M1; Henk's Hollow Site: F57472, right dentary with p2-3, m1-2; F57473, right dentary with p2-3; F57474, left dentary with m1-4; Inabeyance Site: F57438, right dentary edentulous; F57439, left dentary with p2-3, m2-4; Jim's Carousel Site: F24652, crushed skull with right P3, M1-2; Judith's Horizontalis Site: F30546, left maxilla with P3, M1-4; F50657, left maxilla with M3-4; Leaf Locality: UCMP 108542, right M1; QM F57354, left dentary edentulous; Main Site: F57462, left M1; Mike's

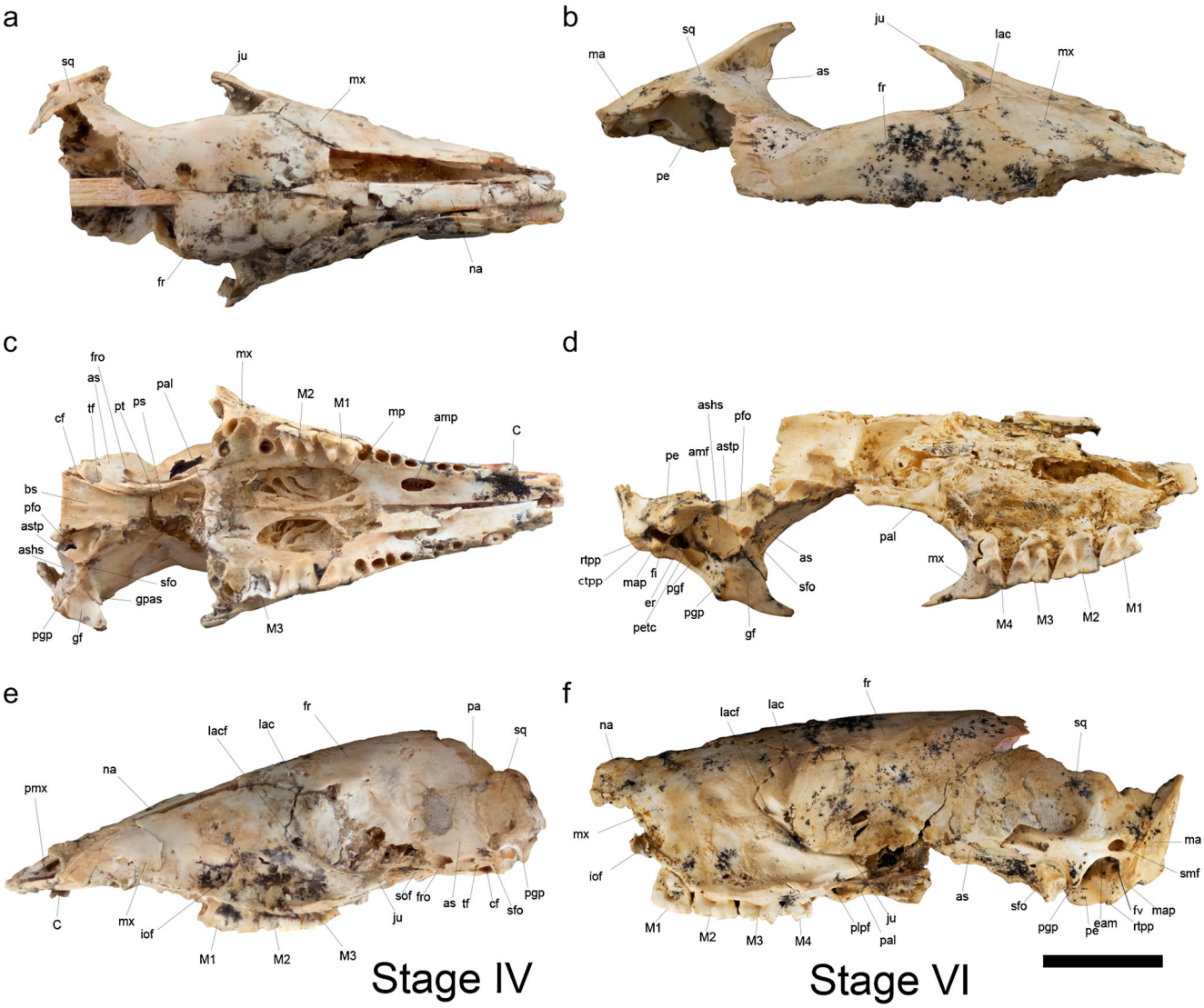

Fig. 3 *Madju variae,* gen. et sp. nov., adult skulls, paratype QM F23405 (**a**, **c,** and **e**), stage IV of ontogenetic series and paratype QM F23406 (**b**, **d,** and **f**), stage VI of ontogenetic series. **a-b**, dorsal view of skulls; **c-d**, ventral view of skulls; **e-f**, left lateral view of skulls. **Abbreviations**: **ctpp**, caudal tympanic process of the petrosal; **er**, epitympanic recess; **fi**, fossa incudus; **fv**, fenestra vestibule; **map**, mastoid process; **petc**, petrosal crest; **pgf**, postglenoid foramen. For all other abbreviations, refer to Fig. 1. Scale bar equals 1 cm

Menagerie Site: F57470, left M3; F57471, left M2; Neville's Garden Site: F23800, partial skull with left P1-3, M1, right P2-3, M1-2; F23805, partial skull with right M3-4, left M2-4; F24241, right maxilla with M2-3; F30697, left dentary with m2-4; F36228, left dentary with m3-4; F36337, associated dentaries with left p1, m2-4, right p1-3, m1; F57399, left dentary with p3, m1-4; F57400, right dentary with p3, m1-4; F57401, left dentary with p2-3, m1-3; F57402, left dentary with m1-4; Phil's Phenomenal Fissure Fill (PPFF) Site: F57467, right dentary with p3, m1, broken m2; F57468, left maxilla with M3-4; Price Is Right Site: F57460, left dentary with p1; F57461, right dentary with p3, m2; Quantum Leap Site: F50791, right dentary with m2-4; F50803, left maxilla with M1-4; Rick's Sausage Site: F56249, left M1; F57451, right M2; F57452, right m3; F57453, right m1; F57454, left m2; F57455, left m2; F57456, right m2; F57457, left m2; F57458, left m1; F57459, left m1; Ringtail Site: F57464, left dentary with m1-3; Ross Scott-Orr (RSO) Site: F57432, left dentary with m2-4; F57433, partial skull with right M1, left C, M1-4; F57434, left maxilla with M1-2; F57435, right maxilla with M1-2; F57436, left M3 and right M2; Two Trees Site: F57463, left dentary with m1-4; Upper site: F57403, right maxilla with P1-3, M4; F57404, Left dentary with p3, m1-3; F57405, right dentary with broken m3, m4; F57407, right dentary with c, p1; F57408, right dentary with p1, p3, m1-4; F57409, right dentary with m3; F57410, left maxilla with M1-3; F57411, right dentary with c, p1-2; F57412, right dentary with c, p1-3, m1-4; F57413, right dentary with c, p2-3, m1; F57414, right dentary with p2-3, m1-4; F57415, right dentary with m4; F57416, left dentary with m2; F57417, right M2;

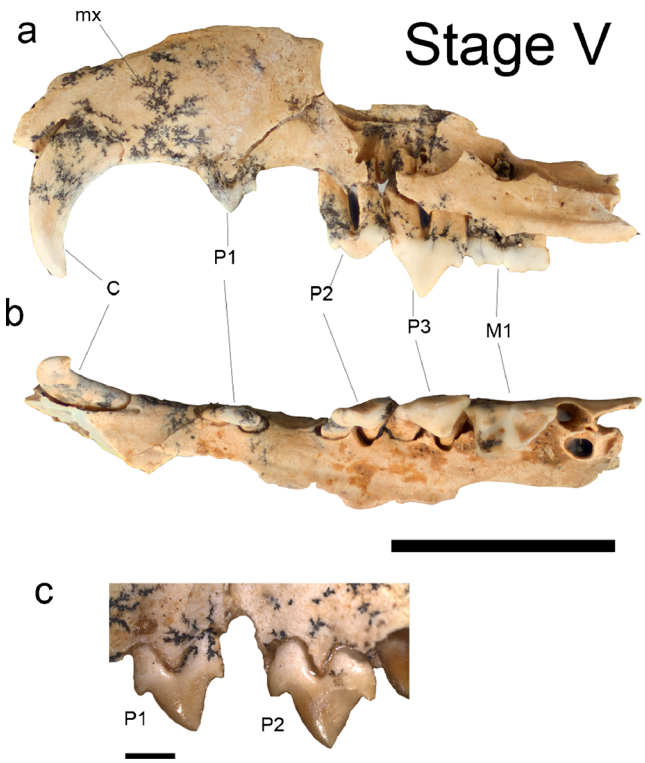

Fig. 4 *Madju variae,* gen. et sp. nov., paratype QM F23430 (**a** and **b**), left maxilla with C, P1-3, M1, stage V of ontogenetic series and paratype QM F57324 (**c**), left P1 and P2. **a,** left lateral view of maxilla; **b**, ventral view of maxilla; **c**, buccal view of left P1 and P2. For abbreviations, refer to Fig. 1. Scale bar equals 1 cm for **a** and **b**, 1 mm for **c**

F57418, left dentary with p3, m1-4; F57419, left dentary with m3; F57420, left dentary with broken m2, m3-4; F57421, left maxilla with M3-4; F57422, right maxilla with M1-3; F57423, left maxilla with M2; F57424, right maxilla with M1; F57425, right dentary with m1-2; F57426, right maxilla with M1-2; F57427, left dentary with c, p1-3; F57428, left maxilla with P2-3, M1-2; F57429, left dentary with m2-3; F57430, left maxilla with M3; F57431, left maxilla with M3-4; VIP Site: F24419, left dentary with p1-3 m1-4; Wang Site: F57466, left dentary with p3, m1-4; Wayne's Wok Site: F23554, left maxilla with P3 unerupted, M1-2; F24312, right maxilla with M1; F24420, right dentary c, p1-2, m2-4; F36361, left dentary with p1; F36362, left dentary with p2-3, m1-3; F39853, left dentary with c, p2, m1-4; F57380, right dentary c, p1, m3-4; F57381, left dentary with m2-4; F57382, right dentary with m4; F57383, left dentary with m1-4; F57384, left dentary with p1 and p3; F57385, right dentary, c, p1-3, m4; F57386, right dentary with m2-4; F57387, left dentary with m2; F57388, left dentary with p1-2, m4; F57389, right maxilla with P2-3, M1-2; F57390, right dentary with m4; F57391, left dentary with m2-3; F57392, left dentary with m3; F57393, right dentary with broken c,p1-3, m1; F57394, left dentary with m1-4; F57395, left dentary with m3; F57396, right dentary with m3-4; F57397, left maxilla with M2-3; White Hunter Site: F57559, right dentary with p2; F57560, isolated right m2-3; F57561, left dentary with p3.

Type Locality The holotype F57323 and paratype F57379 are from Wayne's Wok Site; paratype F23405 is from Inabeyance Site; paratypes F23406, F23429, F23430, F23431, and F24227 are from Camel Sputum Site; paratype F24328 is from Neville's Garden Site; paratype F57322 is from Upper Site; paratypes F36336, F57321, F57324, and F57437 are from AL90 Site; Riversleigh World Heritage Area, northwestern Queensland. Precise locality details have been lodged with the Queensland Museum.

Age and Stratigraphy The White Hunter Local Fauna is part of Faunal Zone A, and the Wayne's Wok, Inabeyance, Camel Sputum, Neville's Garden, Upper Site, Cadbury's Kingdom, Creaser's Ramparts, Dirk's Towers, Judith's Horizontalis, Mike's Menagerie, Price Is Right, Quantum Leap, RSO, and VIP Local Faunas are part of Faunal Zone B, estimated to be approximately late Oligocene and early Miocene in age, respectively (Archer et al. 1997; Arena 2004; Travouillon et al. 2006, 2011, 2013a). The Kutjamarpu LF from the Leaf Locality in the Tirari Desert, South Australia, is estimated to be approximately early Miocene in age (Archer et al. 1997; Travouillon et al. 2006). The AL90, Gag, Golden Steph, Gotham City, Henk's Hollow, Jim's Carousel, Main Site, Rick's Sausage, Ringtail, Two Trees, and Wang Local Faunas are part of Faunal Zone C, estimated to be approximately middle Miocene in age (Archer et al. 1997; Arena 2004; Travouillon et al. 2006, 2011, 2013a). The age of the Phil's Phenomenal Fissure Fill LF is unknown.

Specific Etymology Variae from Latin "varius" meaning various or a number of types, in reference to its dimorphic nature.

Specific Diagnosis Madju variae differs from *Madju encorensis* in having the following features: stylar cusp D1 present on M1; stylar cusp B visible on M1 as a distinct cusp; stylar crest present on M2, but not connected to stylar cusp D; stylar cusp B on M3 is conical with no associated crest; preparacrista connects to stylar cusp A on M3; stylar cusp E present on M3 as a small remnant; no anterior cingulid is present on m1; posthypocristid is oblique to the tooth row on m4.

Description

Skull The description of the skull of *M. variae* is based on the holotype QM F57978, and paratypes F23405, F23406, F36336, and F57321.

The skull is relatively long-snouted compared to other fossil species such as those of *Galadi, Yarala,* and *Bulungu*

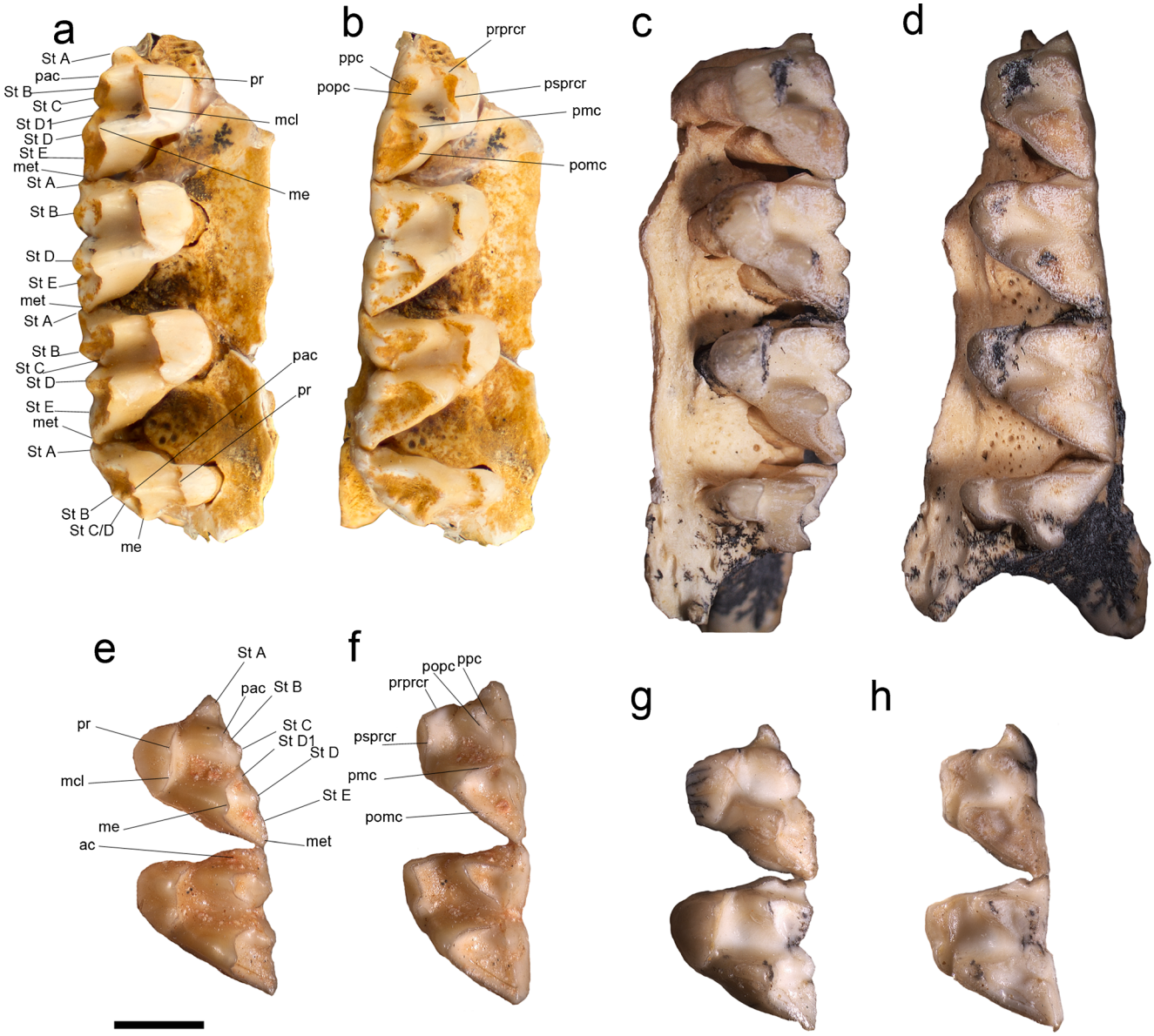

Fig. 5 *Madju variae,* gen. et sp. nov., upper molars. **a**, lingual view of right M1-4 (paratype QM F57322); **b**, occlusal view of right M1-4 (paratype QM F57322); **c**, lingual view of left M1-4 (paratype QM F23429); **d**, occlusal view of left M1-4 (paratype QM F23429); **e**, lingual view of left M1-2 (paratype QM F57321); **f**, occlusal view of left M1-2 (paratype QM F57321); **g**, lingual view of left M1-2 (paratype QM F23405); **h**, occlusal view of left M1-2 (paratype QM F23405). **Abbreviations**: **ac**, anterior cingulum; **mcl**, metaconular hypocone; **me**, metacone; **met**, metastyle; **pac**, paracone; **pmc**, premetacrista; **pomc**, postmetacrista; **popc**, postparacrista; **ppc**, preparacrista; **pr**, protocone; **prprcr**, preprotocrista; **psprcr**, postprotocrista; **StA-E**, stylar cups A to E. Scale bar equals 2 mm

but less so compared to extant species of *Perameles, Echymipera,* and *Peroryctes.* The rostrum is narrow anteriorly and tapers gradually in dorsal view (Figs. 1, 2, and 3). Most sutures, if not damaged or absent, are visible. The premaxilla is only partially preserved in QM F57978 (Fig. 1), F57321 (Fig. 2), and F23405 (Fig. 3). The premaxillary-maxillary suture occurs just to the anterior edge of the canine alveolus, which is confined to the maxilla. The lateral surface of the maxilla is flat, with very little swelling caused by the canine root. The infraorbital foramen is located at a level above the anterior root of M1. The shallow antorbital fossa is present posteriorly above M3 and M4 in adults (F23405, F23406; Fig. 3) but more anteriorly in juveniles (above M2-3 in F57978 and F57321, above M1-2 in F36336; Figs. 1, and 2). The maxillary/jugal suture is V-shaped (posteriorly pointed) on the zygomatic arch around the antorbital fossa. The nasofrontal suture is saw-edged and terminates posteriorly at a point anterior to the anterior region of the antorbital fossa.

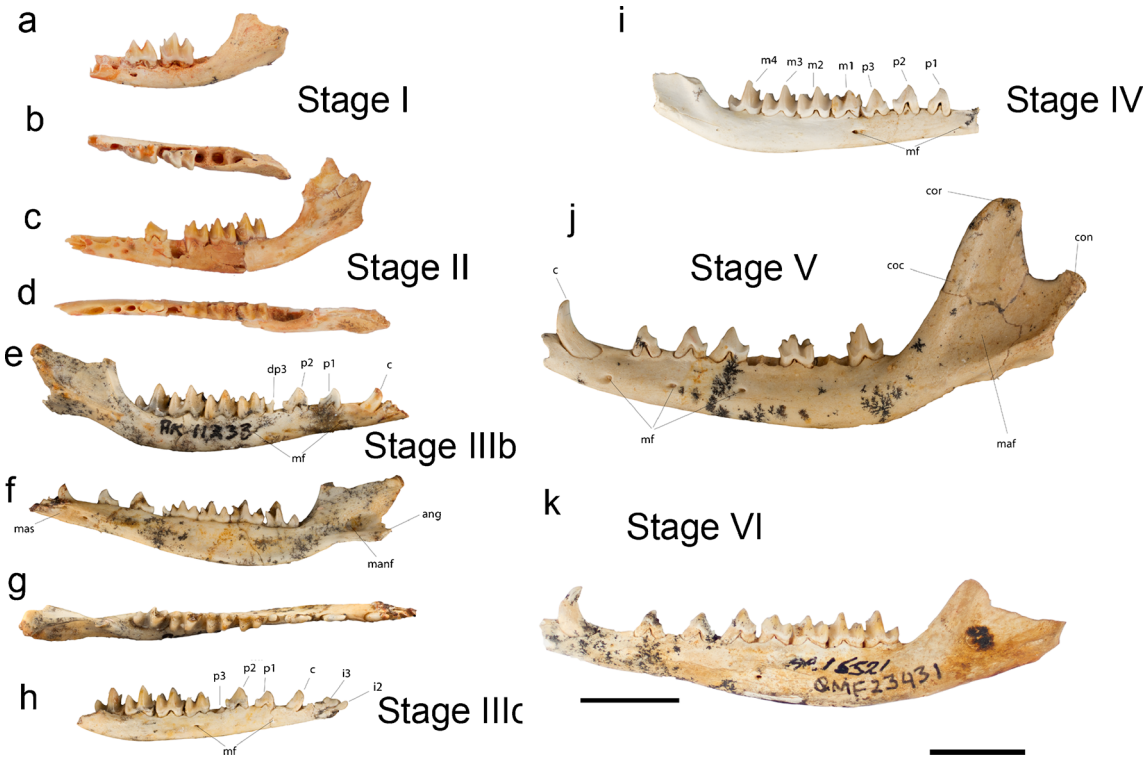

Fig. 6 *Madju variae,* gen. et sp. nov., dentaries. **a**, buccal view of juvenile left dentary with m1-2 (Stage I, paratype QM F24328); **b**, occlusal view of juvenile left dentary with m1-2 (Stage I, paratype QM F24328); **c**, buccal view of juvenile left dentary with p2, m1-3 (Stage II, paratype QM F57321); **d**, occlusal view of juvenile left dentary with p2, m1-3 (Stage II, paratype QM F57321); **e**, buccal view of juvenile right dentary with c, p1-2, dp3, m1-4 (Stage IIIb, paratype QM F57979); **f**, lingual view of juvenile right dentary with c, p1-2, dp3, m1-4 (Stage IIIb, paratype QM F57979); **g**, occlusal view of juvenile right dentary with c, p1-2, dp3, m1-4 (Stage IIIb, paratype QM F57979); **h**, buccal view of juvenile right dentary with i2-3, c, p1-3, m1-4 (Stage IIIc, paratype QM F57437); **i**, buccal view of right adult dentary with p1-3, m1-4 (Stage IV, paratype QM F24227); **j**, buccal view of adult left dentary with c, p1-3, m2, m4 (Stage V, paratype QM F57323); **k**, buccal view of left adult dentary with c, p1-3, m1-4 (Stage VI, paratype QM F23431). **Abbreviations**: **coc**, coronoid crest; **i2-3**, lower incisor 2 and 3; **manf**, mandibular foramen. For all other abbreviations, refer to Fig. 1. Scale bar equals 1 cm

Nasals are uniform in thickness along the majority of their length, and narrow. The posterior contact of both nasals with the frontals forms an angle less than 90° (Fig. 1). The maxillary-frontal suture extends anteromedially from the anterior corner of the lacrimal. There is small extension of the lacrimal onto the facial region of the snout. The lacrimal foramen is located very close to the maxillary-lacrimal suture and is isolated from the maxilla by a thin extension of the lacrimal. No crest is developed in the lacrimal. The facial-orbital boundary in the lacrimal is poorly defined by the gently curved lacrimal. The lacrimal is ovoid in shape, thinning ventrally within the orbit. The lacrimal lines the dorsal and lateral walls of the maxillary foramen (the posterior opening of the infraorbital canal). The frontal extends as a small pointed flange into this foramen on the medial side (Figs. 1, 2, and 3). The sphenopalatine foramen occurs low in the orbit, just dorsal to the frontal-maxillary suture. A smaller, ovoid caudal palatine foramen lies directly below the sphenopalatine foramen and ventrally is bound by both the maxilla and palatine.

Posterior extensions of the incisive foramina intruding into the anterior edge of the maxillae are present in the palate of juvenile skulls (F36336 and F57321; Fig. 2). A pair of accessory palatal fenestrae, sensu Voss and Jansa (2003), are present, separated by a well-developed septum. These accessory palatal fenestrae extend from the level of the anterior edge of the alveolus for P1 to a point level with the middle of P2 in F36336 and F57321 (Fig. 2). They are smaller in the holotype QM F57978 (posterior alveolus of P1 to anterior alveolus of P2; Fig. 1) and paratype F23405 (posterior of P1 alveoli to middle of P2; Fig. 3). A set of maxillopalatine fenestrae are present posterior to the accessory palatal fenestrae and are larger (except for F36336; Fig. 2) with thinner dividing septum (Fig. 3). They extend from a point level with the middle of P3 to a point level with the posterior edge of M3. The maxillopalatine suture is "N"-shaped with a long thin extension of the palatine entering the maxilla.

The interfrontal suture is straight for the anterior two-thirds of its length, but sinuous for the posterior third (Fig 2). The frontal-parietal suture is sinuous and shows a large degree of

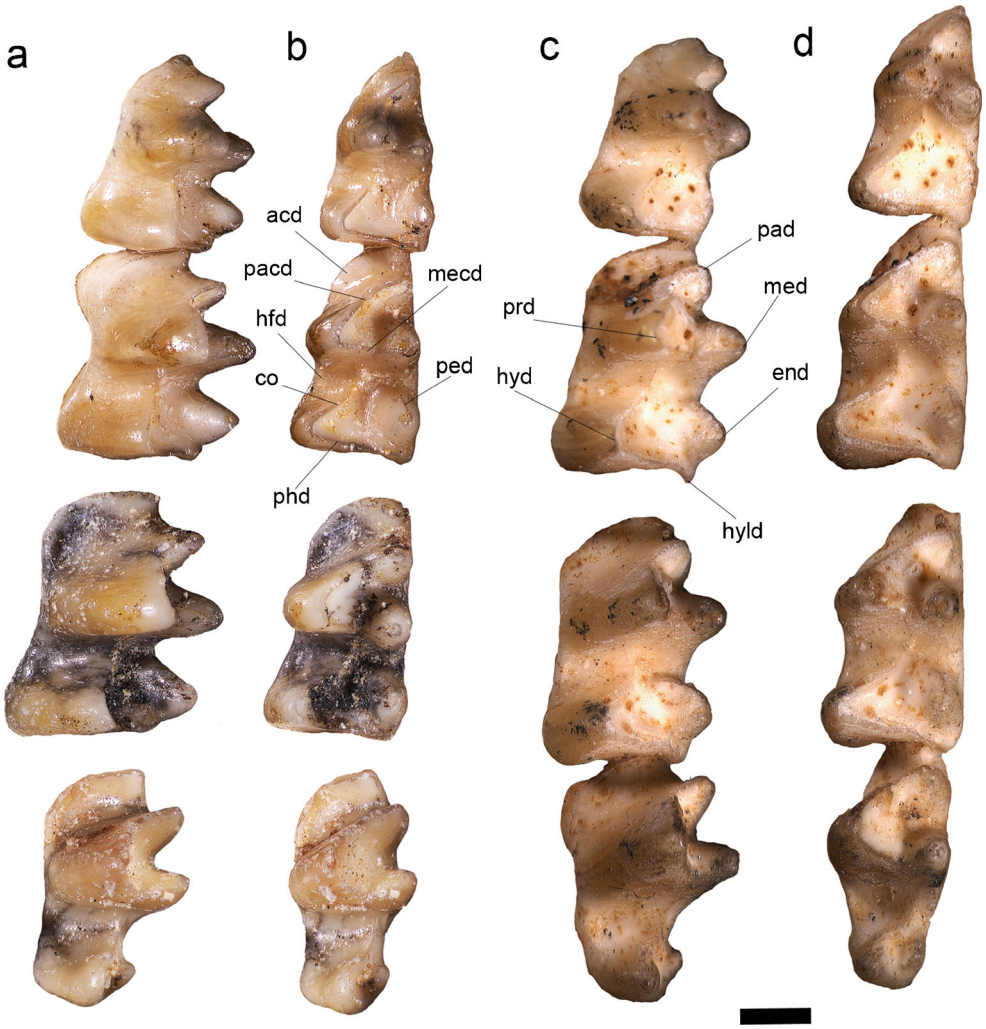

Fig. 7 *Madju variae,* gen. et sp. nov., lower molars. **a**, buccal view of left m1-4 (paratype QM F57437); **b**, occlusal view of left m1-4 (paratype QM F57437); **c**, buccal view of left m1-4 (paratype QM F23431);**d**, occlusal view of left m1-4 (paratype QM F23431). **Abbreviations**: **acd**, anterior cingulid; **co**, cristid obliqua; **end**, entoconid; **hfd**, hypoflexid; **hyd**, hypoconid; **hyld**, hypoconulid; **mecd**, metacristid; **med**, metaconid; **pacd**, paracristid; **pad**, paraconid; **ped**, preentocristid; **phd**, posthypocristid; **prd**, protoconid. Scale bar equals 1 mm

overlap, with the parietal overlying the frontal. The interparietal suture is anteriorly visible but it is posteriorly co-ossified (Fig 2b). The frontal-alisphenoid contact is curved and oblique in the region above the foramen rotundum. The dorsal extension of the alisphenoid is high but not as high dorsally as the squamosal and it does not contact the parietal (Fig 1). The squamosal has a short contact with the frontal. The alisphenoid overlaps the squamosal and forms a straight oblique suture that continues into the zygomatic arch. There is very little mastoid extension onto the lateral side of the skull.

The foramen rotundum is large, tube-like, and located immediately posterior to the sphenorbital fissure (Figs. 1, 2, and 3). The transverse canal foramen is rounded in ventral view and large. The carotid foramen occurs immediately posteromedial to the transverse canal foramen (Figs. 1 and 3). It is separated from the transverse canal foramen by a very thin wall of alisphenoid, although this wall is wider in juveniles (Fig. 2). The basioccipital-basisphenoid suture occurs posterior to the carotid foramen. Posterolateral to the carotid foramen lies the irregularly shaped primary foramen ovale (Figs. 1b, and 3c, d). The primary foramen ovale is much smaller than in *Galadi speciosus* (Travouillon et al. 2010), *Bulungu palara* (Gurovich et al. 2013), or *Yarala burchfieldi* (Muirhead 2000), and it is entirely bounded by the alisphenoid. Directly lateral to the primary foramen ovale, there is a secondary foramen ovale that is represented by a tunnel formed by an overlapping part of the alisphenoid that extends forward from the anterior surface of the alisphenoid tympanic wing. The alisphenoid tympanic wing (Fig. 2c, e) is round in all dimensions, as it is in *Perameles nasuta*. The floor of the alisphenoid tympanic wing is open on the lateral side but well floored medially. The glenoid fossa consists mostly of the squamosal although the glenoid process of the alisphenoid occupies the medial rim (Fig. 3c, d).

The alisphenoid hypotympanic sinus is rounded anteriorly. Posteriorly, an anterior medial flange is present and curves around the posterior edge of the alisphenoid hypotympanic sinus defining its separation from the epitympanic recess. The

alisphenoid hypotympanic sinus roof is made up mostly of alisphenoid with the alisphenoid-petrosal suture running close to the anterior medial flange. The squamosal does not contribute to the roof of the alisphenoid hypotympanic sinus. The postglenoid foramen is larger than the suprameatal foramen (Wible 2003) or subsquamosal foramen of Archer (1976). It is primarily bounded by the squamosal but its medial side is made up of a wall of petrosal.

The petrosal is generally flat with a more bulbous posterior region. A high ridge is present on the promontorium ventrally on the bulbous portion of the petrosal. Posterolateral to this ridge, a small rostral tympanic process of the petrosal is present. The secondary facial nerve foramen is located on the lateral side of the petrosal, very close to the fenestra vestibuli, which is slightly larger and separated by a very thin wall of bone. The fenestra cochleae is ovoid in shape and located at the posterior side of the bulbous promontorium. A deep fossa incudis lies at the posterolateral base of the petrosal. A small but relatively deep epitympanic recess is located between the fossa incudis and the wall of the postglenoid foramen. There is no squamosal epitympanic sinus. However, the squamosal flattens to an almost horizontal surface around the external auditory opening. A well-developed mastoid process is present lateral to the fossa incudis and anterior to the caudal tympanic process of the petrosal. Fenestra vestibuli is ovoid in shape.

Upper Dentition The description of the upper dentition of *M. variae* is based on the holotype QM F57978, and paratypes F23405, F23406, F23430, F23429, F23800, F57321, F57322, F57324, F57359, and F57433. No upper incisors are represented. C1 is short (does not extend ventrally further than the level reached by the molar crowns), transversely thin and ovoid in cross section in F57978, F23405, F23800, F57359, and F57433 but large (extends ventrally past the level reached by the molar crowns) and wide in F23430 (Fig. 4). This is consistent with the plesiomorphic condition in peramelemorphians where males have significantly larger canines than females, except in species of *Peroryctes, Microperoryctes, Echymipera* (except *E. clara*), and *Chaeropus,* which have, as a derived feature, small canines in both genders. C1 is obliquely angled in the maxilla and sharply recurved along the crown length. Enamel covers only the tip of the canine with dentine as the surface of the tooth for the remaining two-thirds of the crown length. The C1 alveolus is formed within the maxilla only. A large diastema occurs between the C1 and P1 (Fig. 4).

The premolars increase in size posteriorly (Fig. 4). All have an anterior and posterior cusp in addition to the large central cusp. These are small on P1 and increase in size posteriorly. P1 is recurved. The main cusp is anteriorly situated on the crown but is centrally located between the two roots because of the crown's reclination. There is no anterior crest but a short posterior crest is present. The crown of P1 is linear with no lateral expansion. A long diastema is present between P1 and P2. P2 and P3, in contrast, have centrally located main cusps. P3 widens posteriorly and has a small lingual cingulum. The posterior root of P1-3 is wider than the anterior root, with roots exposed in older individuals (e.g., F23430; Fig. 4a).

The buccal length of M1 is greatest followed by posterior, anterior, and lingual dimensions (Fig. 5). Stylar cusp A is present at the most anterobuccal edge of the tooth, as a tall distinct cusp. The anterior cingulum is present just lingual to stylar cusp A as a triangular extension of enamel but at a much lower level and does not connect to the preprotocrista (Fig. 5). The paracone is located posterolingual to stylar cup A, and connected to the small stylar cusp B by the preparacrista, which runs first perpendicular to the tooth row before continuing obliquely through stylar cusp B, and connecting posterobuccally to the much taller stylar cusp C (sensu Travouillon et al. 2013b). In specimens from Faunal Zone C (e.g., F57321, Fig. 5), stylar cusp B is much reduced and barely visible above the preparacrista, which runs obliquely from the paracone to stylar cusp C. The preparacrista continues through the oval stylar cusp C and ends at its posterior edge. The postparacrista runs posterobuccally to the lingual base of stylar cusp C and does not join the premetacrista. Stylar cusp D is the tallest cusp on the crown and oval in shape. It is anteroposteriorly extended in width by adjoining to small, indistinct cusps on either side, stylar cusp D1 and stylar cusp E. A crest runs through these stylar cusps and continues to the posterobuccal corner of the crown. No crest connects stylar cusp C and stylar cusp D1; a short valley is present between these two cusps. Premetacrista termination is variable, ending at the lingual flank of stylar cusps D1 or D (Fig. 5). The metacone is located lingual to stylar cusp D and extends lingually further than the paracone. The postmetacrista is the longest crest on the crown, followed (in decreasing length) by the premetacrista, preparacrista, postparacrista, postprotocrista, preprotocrista, and crests around the metaconular hypocone. The protocone is located posterolingual to the paracone and anterolingual to the metacone. The postprotocrista terminates on the posterolingual flank of the metacone. The posterior cingulum is absent. The metaconular hypocone lies lingual to the metacone and directly posterior to the protocone. Crests around the trigon basin produce a very low 'W.' The surface area in the trigon basin is both wide and long, with almost equal distance between the paracone, metacone, and protocone.

The morphology of M2 follows that of M1 except as follows (Fig. 5). The anterior cingulum is notched and wider in lingual-buccal direction. Stylar cusp A is higher than on M1. Stylar cusp B is the tallest cusp on the stylar shelf and more anteriorly located and almost directly buccal to the paracone. Stylar cusps C and D1 are absent. The paracone is

more lingually located, therefore closer to the metacone. This lingual position of the paracone results in a greater length of both the preparacrista and postmetacrista. The anterior position and size of stylar cusp B have resulted in an additional crest along the stylar shelf. The anterobuccal region of the crown therefore is triangular rather than linear in shape. Stylar cusp D is smaller than stylar cusp B followed (in decreasing height) by stylar cusp E, metastyle, stylar cusp A, metacone, paracone, protocone, and metaconular hypocone. The protocone is more lingually positioned than on M1 but the metaconular hypocone is equally distant from the metacone as on M1. The protocone therefore is anterolingual to the metaconular hypocone. All crests on the crown are elongate.

The morphology of M3 follows that of M2 except as follows (Fig. 5). The preparacrista joins stylar cusp A rather than stylar cusp B (as on M1 and M2). Stylar cusp A is almost as high as stylar cusp B. The small stylar cusp C is present in the valley between stylar cusps B and D. The postparacrista terminates at the lingual flank of stylar cusp C. Stylar cusp E is not connected to stylar cusp D by a crest. Stylar cusp E is minute but distinct. Stylar cusps B and D are conical with no crest running through them. Stylar cusp D is high with stylar cusp B only slightly lower. The paracone is more lingually located, almost directly anterior to the metacone. The protocone is slightly more lingual than on M2. The ectoflexus is more extreme than on the previous molars. The buccal flank is not parallel to the tooth row. Both the anterior and posterior buccal flanks curve inwards with an additional central curve around stylar cusp D. The angle between the crests at the protocone and metaconular hypocone is sharper.

The morphology of M4 follows that of M3 except as follows (Fig. 5). The paracone is larger and more lingually positioned. Stylar cusp B is reduced and more lingually positioned. The metastylar shelf is reduced to the variably-sized metacone, which connects to the paracone via the postparacrista. The angle between the preparacrista and postparacrista is wider than in M3. An ectoflexus is present between stylar cusp B and the metacone in all specimens except F57322 (Fig. 5) where a stylar cusp is present in its place (probably stylar cusp C or D). Stylar cusp A is the highest cusp on the crown, followed in decreasing order by stylar cusp B, paracone, stylar cusp C/D (if present), metacone, and protocone. No metaconular hypocone is present. The talon basin is reduced, with the postprotocrista ending at the lingual flank of the postparacrista, midway between the paracone and metacone.

Dentary The description of the dentary and lower dentition of *M. variae* is based on the holotype QM F57978, and paratypes F23405, F23431 F24227, F24328, F57321, F57323, F57324, F57379, and F57437. The ramus is generally thin and uniform in width along most of its length (Fig. 6), although it is more robust in some specimens, which are likely to be male, having correspondingly enlarged canine (e.g., F23431, F20890, F29705, F57323, F57361, F23724, and F57413). The greatest thickness of the dentary is beneath m3, although this region is not much thicker than the remainder of the dentary. Mental foramina are present: one large between the roots of c1 and p1 (more posteriorly situated below the anterior root of p1 in juveniles) and a smaller one below the roots of m1 (position varies with age, below the posterior root of m1 in juveniles, and below the anterior root of m1 in adults). Additional mental foramina are present in F57323, below the anterior root of p2. The coronoid process departs from the ramus at around 100°. The mandibular condyle is higher than half of the coronoid height. The masseteric fossa is shallow. The mandibular foramen is large and lies in the corner between the coronoid and angular processes. The mandibular symphysis extends as far as the anterior root of p2.

Lower Dentition The crown of i1 is not preserved in any specimen. The arrangement of the i1 root and alveolus indicate i1 and i3 emerge dorsal to the level of i2 (Fig. 6). The i2 is unicuspid, small with a rounded anterior edge. The crown of i3 is bilobed with the posterior lobe small and dorsally-orientated. The anterior lobe is directed anteriorly and follows the direction of the tooth row. A small diastema is present between i3 and c1.

The canine is large in more robust specimens (e.g., F23431 and F57323; Fig. 6). Crown height exceeds that of p3. The canine is obliquely angled, recurved with enamel confined to the tip of the crown. In more gracile specimens (e.g., F57437, F57380, F57384), the canine is slightly smaller in all dimensions and does not exceed the crown height of p3.

A diastema is present between the canine and p1, shorter than p1 in juveniles, but as long or longer in adults (Fig. 6). The p1 crown is crescent-shaped in dorsal view. In occlusal view, the crown is as wide anteriorly as it is posteriorly. The main cusp is located anterior to the centre, connected to the posterior cusp by a long trailing crest. Neither the anterior cusp nor cingula is present. Roots are exposed with age and recline posteriorly in older individuals (Fig. 6).

A short diastema is present between p1 and p2 (Fig. 6). The p2 is similar to p1 in morphology except as follow: the main cusp and posterior cusp are taller and wider; a small anterior cusp present; and in occlusal view, the tooth is wider and longer, oval in shape, wider posteriorly than anteriorly.

No diastema separates p2 and p3. The p3 is similar to p2 in morphology except as follows: in occlusal view, the tooth is longer and wider; the main cusp is taller and wider; the anterior cusp is more prominent; the tooth reclines more posteriorly with age; and a shallow basin or cingulum is developed on the buccal side.

No anterior cingulum is present on m1 (Fig. 7). The protoconid is closer to the metaconid than paraconid and positioned anterobuccal to the metaconid. The paraconid lies

slightly anterobuccal to the metaconid. In unworn teeth (Fig. 7), the protoconid is the tallest cusp, followed in decreasing order by the metaconid, entoconid, paraconid, hypoconid, and hypoconulid. In worn teeth (Fig. 7), the metaconid is the tallest, followed by the protoconid, paraconid, entoconid, hypoconid, and hypoconulid. The entoconid is oval in shape, tall, with the preentocristid descending anteriorly from the tip of the cusp and ending at the anterior base of the entoconid. The hypoconulid is distinct and directly posterior to the entoconid. The hypoconulid is connected to the hypoconid by a straight, oblique posthypocristid. The cristid obliqua is straight and terminates level with the midpoint of the metacristid. A small hypoflexid is present.

The morphology of m2 is similar to that of m1 except as follows. In occlusal view, the tooth is longer and wider. The metaconid is directly lingual to the protoconid, and the paraconid lies directly anterior to the metaconid. The metaconid-paraconid distance is shorter than metaconid-protoconid distance. The anterior cingulum is present, thick, and terminates at the base of protoconid. The entoconid is taller and wider. The hypoconid is positioned more anteriorly, almost directly buccal to the entoconid. The cristid obliqua is slightly concave in occlusal view. The hypoflexid is larger. The protoconid extends buccally but not as much as the hypoconid. The metaconid is the largest cuspid on the tooth followed (in decreasing height) by the protoconid, entoconid, paraconid, hypoconid, and hypoconulid. The posthypocristid is the longest crest on the tooth followed (in decreasing length) by the paracristid, metacristid, cristid obliqua, and preentocristid.

The morphology of m3 is similar to that of m2 except as follows. The tooth is longer and wider in occlusal view. The anterior cingulum is longer and wider. The protoconid is buccally shifted almost to the level of the hypoconid. The hypoflexid is further enlarged. The hypoconid is buccally shifted, directly buccal to the entoconid. In QM F57437, the hypoconulid is reduced and the posthypocristid joins this cusp to the hypoconid at an angle perpendicular to the tooth row. In F23431, the size of the hypoconulid and the direction of the posthypocristid are similar to the condition in m2.

The morphology of m4 is similar to that of m3 except as follows. The tooth is longer but not as wide. The protoconid is more lingually positioned. The paraconid is larger, but more anteriorly positioned, increasing the distance between the paraconid and metaconid, but remaining shorter than the metaconid-protoconid distance. The talonid is reduced in size. The entoconid is smaller than the hypoconid but remains distinct and taller. The cristid obliqua is shorter, concave, and ends lingual to the midpoint of the tooth width. The posthypocristid departs from the hypoconid obliquely, and ends just posterior to the entoconid, with a remnant of the hypoconulid present (e.g., F23431; Fig. 7). The hypoflexid is larger and ends at the buccal side of the hypoconid.

Measurements of the dentitions of *M. variae* are presented in Appendices 1 and 2.

Madju encorensis, sp. nov. (Figs. 8, and 9)

Holotype: QM F57350, right M3.

Paratypes: QM F57330, right m1; F57331, right m2; F57339, right m3; F57345, right M1; F57347, right M2; F57351, right M4; F57353, right m4.

Referred Material QM F57325, right m4; F57326, left m4; F57327, left m4; F57328, left m4; F57329, broken left m4; F57332, right m2; F57333, right m3; F57334, left m3; F57335, left m3; F57336, left m3; F57337, right m3; F57338, right m2; F57340, right m2; F57341, left M1; F57342, left M1; F57343, left M1; F57344, left M1; F57346, broken right M1; F57348, left M2; F57349, broken left M2; F57352, left M4.

Type Locality Encore Site, Riversleigh World Heritage Area, northwestern Queensland.

Age and Stratigraphy Encore Site is part of Faunal Zone D, estimated to be late middle or early late Miocene in age (Archer et al. 1997; Arena 2004; Travouillon et al. 2006, 2011).

Species Etymology Named after the Riversleigh type locality, Encore Site.

Specific Diagnosis Madju encorensis differs from *M. variae* in having the following features: stylar cusp D1 is absent on M1; stylar cusp B is not visible on M1 as a distinct cusp; stylar crest is absent on M2; stylar cusp B on M3 is oval with associated crest; the preparacrista connects to stylar cusps A and B on M3; stylar cusp E is absent on M3; anterior cingulid is present on m1; posthypocristid is perpendicular to the tooth row on m4.

Description

Upper Dentition M1 is longer than wide (Fig. 8). Stylar cusp A is the most anteriorly positioned cusp and lies below the level of the parastylar shelf. A small anterior cingulum is present lingual to stylar cusp A, and ends level with the paracone. The paracone is large and conical, positioned posterolingual to stylar cusp A. A weak preparacrista joins the paracone posterobuccally to the small, conical stylar cusp C; there is no evidence of stylar cusp B. The postparacrista runs parallel to the preparacrista and ends at the lingual flank of stylar cusp C. The preprotocrista terminates anterolingual to the paracone. There is no continuous anterior cingulum. The postprotocrista terminates at the base of the lingual flank of the metacone after diverging around the metaconular hypocone. There is no posterior cingulum. The metacone is the highest

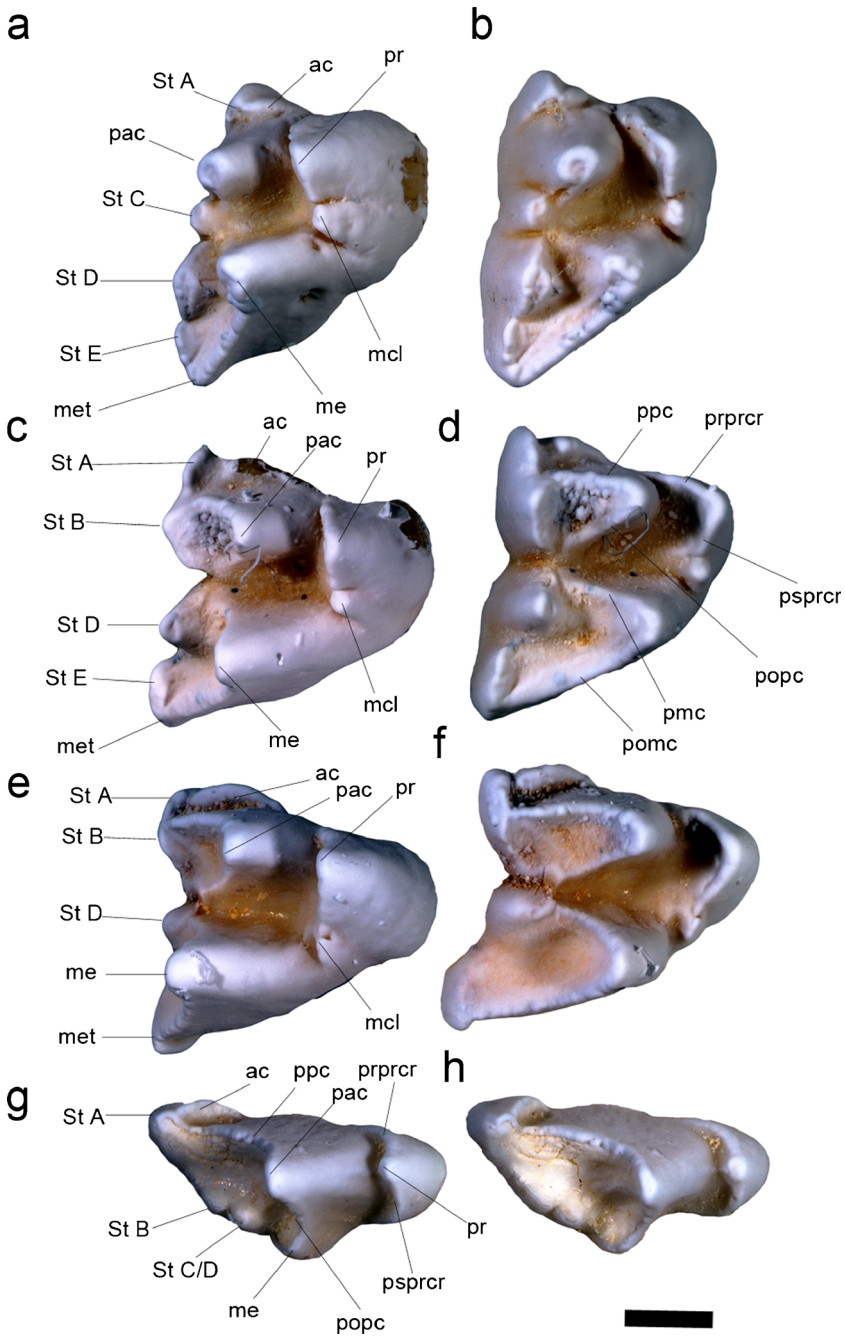

Fig. 8 *Madju encorensis,* gen. et sp. nov., upper molars. **a**, lingual view of RM1 (paratype QM F57345); **b**, occlusal view of RM1 (paratype QM F57345); **c**, lingual view of RM2 (paratype QM F57347); **d**, occlusal view of RM2 (paratype QM F57347); **e**, lingual view of RM3 (holotype QM F57350); **f**, occlusal view of RM3 (holotype QM F57350); **g**, lingual view of RM4 (paratype QM F57351); **h**, occlusal view of RM4 (paratype QM F57351). For all abbreviations, refer to Fig. 5. Scale bar equals 1 mm

cusp on the crown followed (in decreasing height) by stylar cusp D, stylar cusp E, paracone, stylar cusp C, stylar cusp A, protocone, and metaconular hypocone. The premetacrista runs obliquely from the metacone to the anterolingual flank of stylar cusp D. The protocone is situated directly lingual to the paracone. The paracone extends lingually only half as far as the metacone. Stylar cusp D is positioned directly buccal to the metacone. Stylar cusp D is wide but low, with an anterior and posterior crest. Stylar cusp E is present as a tall cusp directly posterior to stylar cusp D. The buccal edge of the tooth smoothly curves to the tips of the stylar cusps, which are not situated on the buccal edge of the crown.

The morphology of M2 is similar to that of M1 except as follows (Fig. 8). Stylar cusp A is higher and a notch is present between stylar cusp A and the anterior cingulum. The anterior cingulum is larger in all dimensions. Stylar cusp B is present and large, almost equal in height to stylar cusp D. Stylar cusp B is directly posterior to stylar cusp A, oval in shape, with a blade running through it anteroposteriorly. The preparacrista is oriented perpendicular to the tooth row and connects with

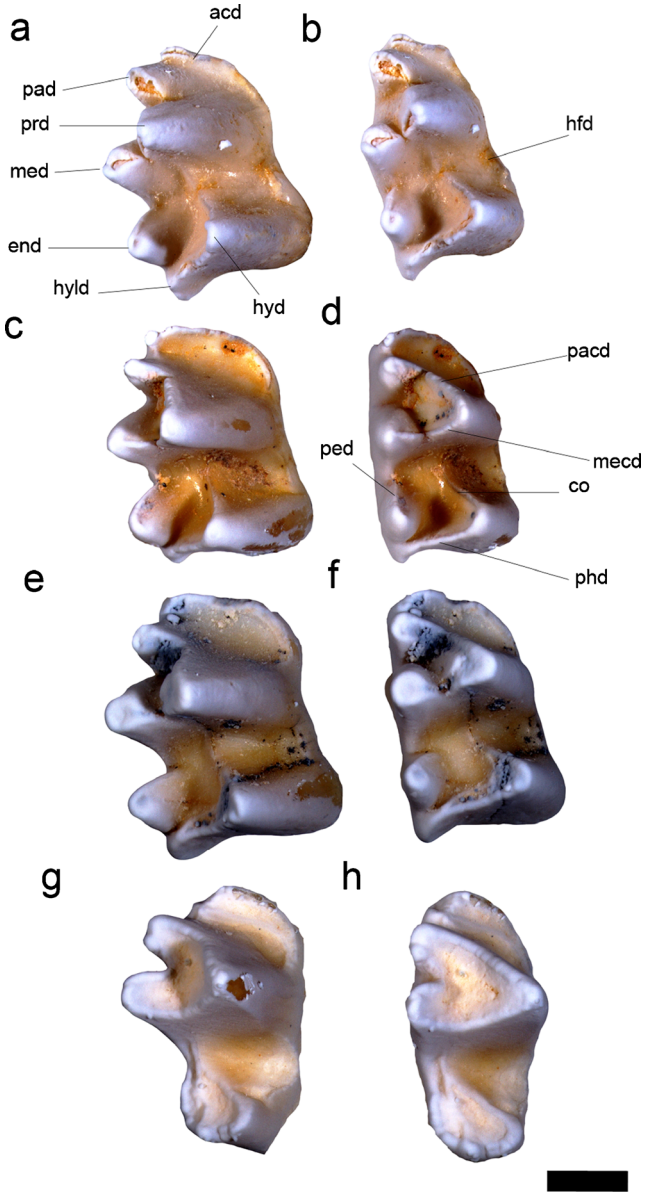

Fig. 9 *Madju encorensis,* gen. et sp. nov., lower molars. **a**, buccal view of Rm1 (paratype QM F57330); **b**, occlusal view of Rm1 (paratype QM F57330); **c**, buccal view of Rm2 (paratype QM F57331); **d**, occlusal view of Rm2 (paratype QM F57331); **e**, buccal view of Rm3 (paratype QM F57339); **f**, occlusal view of Rm3 (paratype QM F57339); **g**, buccal view of Rm4 (paratype QM F57353); **h**, occlusal view of Rm4 (paratype QM F57353). For all abbreviations, refer to Fig. 7. Scale bar equals 1 mm

stylar cusp B. The paracone is not conical and is more lingually positioned. The postparacrista runs posterobuccally to the posterolingual flank of stylar cusp B. A strong cleft is present between stylar cusp B and stylar cusp D. Stylar cusp D is conical and unbladed. Stylar cusp E is present and located posterobuccal to stylar cusp D, with a short crest connecting it to the metastyle. The metacone is enlarged and more lingually positioned, elongating both the premetacrista and postmetacrista. The protocone is more lingually positioned, resulting in the angle between the crests leaving the protocone being smaller.

The morphology of M3 is similar to that of M2 except as follows (Fig. 8). Stylar cusp E is absent. No crests are present between the metastyle and stylar cusp D. The metacone is more lingually positioned elongating both the premetacrista and postmetacrista. Stylar cusp B is more anteriorly positioned and smaller in size. The preparacrista runs directly to the crest that joins both stylar cusps B and A, and continues posteriorly in a 'S' shape before connecting back with the postparacrista, just anterolingual to stylar cusp D. The paracone is lingually positioned to lie level with the metacone. The preparacrista and postparacrista accordingly are lengthened. The protocone is more lingually positioned. The metaconular hypocone is reduced in size.

The morphology of M4 is similar to that of M3 except as follows (Fig. 8). The anterior cingulum is reduced. The paracone is larger and the preparacrista connects to the large stylar cusp A. Stylar cusp B is small, and more posterolingually positioned, with a small crest running through it that does not, however, connect to stylar cusp A. Instead, it is connected to another cusp directly posterolingual to it that is either stylar cusp C or D. The metastylar shelf is absent. The metacone is directly posterobuccal to the paracone, and connected to this cusp via a straight postparacrista. The protocone is reduced and more buccally positioned. The preprotocrista and postprotocrista are equidistant and end on the anterior and posterior flanks of the paracone, respectively. No metaconular hypocone is present.

Lower Dentition The protoconid is the tallest cusp on m1 (Fig. 9) followed (in decreasing cusp height) by the metaconid, hypoconid, entoconid, paraconid, and hypoconulid. A short anterior cingulum runs from the anterior flank of the paraconid to the anterior flank of the protoconid. The metacristid is shorter than the paracristid, both crests being shorter than distance between the paraconid and metaconid. The metaconid is posterolingual to the protoconid. The entoconid is oval with the preentocristid running anteriorly from its tip and ending at the anterior base of the entoconid. There is no distinct connection with the metaconid. The hypoconulid lies directly posterior to the entoconid. No crests connect these two cusps. The hypoconulid is low lying and not raised above the level of the posthypocristid but directed posteriorly, extending further back than the posthypocristid. The posthypocristid is parallel to the metacristid and oblique to the tooth row. The cristid obliqua is concave near its termination midway between the metaconid and protoconid. The hypoconid lies directly buccal to the entoconid. No posterior cingulum is present.

The morphology of m2 is similar to that of m1 except as follows. The anterior cingulum is large, wide, and uniformly thick. The paraconid is more posterolingually located, directly

anterior to the metaconid. The distance between the paraconid and metaconid is reduced. The distance between the paraconid and protoconid is increased. The protoconid is more buccally located, increasing the distance between it and the metaconid. The paracristid and metacristid are longer and the angle between these crests is smaller. The hypoconid is only slightly more buccally positioned than the protoconid. The posthypocristid is longer than on m1 and less oblique. The cristid obliqua is also slightly longer.

The morphology of m3 is similar to that of m2 except as follows. The anterior cingulum is larger. The protoconid and hypoconid are more buccally positioned with all associated crests lengthened appropriately. The entoconid is slightly more conical.

The morphology of m4 follows that of m3 except as follows. The anterior cingulum is reduced in width on the buccal side. The protoconid is more buccally positioned extending the length of the paracristid and metacristid. The talonid is extremely reduced, but also extremely worn. All crests on the talonid are connected to each other, presumably the result of wear. The hypoconid is more lingually positioned and very small. The posthypocristid is perpendicular to the tooth row. The cristid obliqua terminates at the posterior flank of the metaconid.

Measurements of the dentitions of *M. encorensis* are presented in Appendices 3 and 4.

Results

Qualitative comparisons

For each of the ontogenetic stages identified, suture development, growth, and dental eruption are described and compared to other stages, taking into account that preservation is not equal in each of the skulls examined.

Stage I Several sutures are not completely closed, including the frontal-parietal, frontal-frontal, maxillary-frontal, frontal-nasal, palatine-frontal, parietal-parietal, and all lacrimal sutures (Fig. 2). The accessory palatal fenestrae are large and subequal in size to the maxillopalatine fenestrae. Both fenestrae are irregular in shape. The maxilla is rugose above the alveoli of the molars in lateral view. In dorsal view, no postorbital constriction is present.

The alveoli for C, P1, P2, and dP3 are present, suggesting that these teeth were fully erupted. The crown of M1 is preserved and unworn. The alveoli for M2 are complete. The alveoli for M3 are damaged, but the bone around the alveoli is thin, suggesting that M3 was not fully erupted.

The ramus of the dentary is shallower than the height of m2 throughout its length. A mental foramen is present below the anterior root of m1. The coronoid process departs from the ramus level with the middle of the alveoli for m3. The crowns of p2, m1, and m2 are present and unworn. A single alveolus for dp3 is present anterior to m1. Two fully formed alveoli are present posterior to m2 for a fully formed and erupted m3. An additional alveolus is present posteriorly at a point below which the m4 would have been developing.

Stage II The frontal-frontal, frontal-nasal, and frontal-parietal sutures are fully closed (sinuous sutures), but the maxillary-frontal sutures and lacrimal sutures are not fully closed. In dorsal view, a weak postorbital constriction is present. Palatine-frontal sutures are not preserved in the specimen (Fig. 2). The parietal-parietal sutures are completely fused posteriorly (no suture lines are visible). The parietals are the same size as in Stage I, but the frontals have elongated anteriorly. All posterior sutures seem to have closed or fused, in contrast to the anterior sutures which remain open where bones are still growing.

The accessory palatal fenestrae occupy the same position as in Stage I (from the anterior root of P1 to the middle of P2) but have increased in length and width, and are perfectly oval in shape. The increase in length seems to correlate with the development of a new diastema between the posterior alveolus of P1 and anterior alveolus of P2, this diastema being absent in Stage 1. The area where the width of these accessory palatal fenestrae has increased is less obvious, but the maxilla seems thicker around the fenestra, suggesting that growth occurred throughout the maxilla. The maxillopalatine fenestrae have enlarged in a posterior direction, suggesting that growth occurred close to the palatine-maxillary suture. In lateral view, the maxilla has grown, increasing the distance between the orbital rim and the infraorbital canal, which remains above M1. As the maxilla grows, the antorbital fossa deepens and a vacuity starts to form, exposing part of the anterior root of M2.

Fully developed alveoli are present in the maxilla for M3, suggesting that this tooth was fully formed and erupted. No alveoli for M4 are present, indicating that M4 had not yet erupted.

The ramus of the dentary is twice as deep as in Stage I. Two mental foramina are present below the anterior root of p1 and m1. The coronoid process departs from the ramus level with the middle of the alveoli for m4, suggesting growth of the dentary has been primarily in a posterior direction. A single alveolus remains between p2 and m1 (for a dp3 which presumably was lost prior to fossilisation or fell out of the dentary during the preparation of the fossil), with no evidence of p3 erupting. The m3 is fully erupted, and the alveoli of m4 are partially formed, suggesting that m4 was beginning to erupt. All teeth are unworn.

Stage IIIa: The maxillary-frontal and lacrimal sutures are closed. In dorsal view, a postorbital constriction is well developed. All comparable cranial bones are of similar size as in Stage II except for the maxilla, which has relatively increased in length. In the antorbital fossa region, an additional vacuity is present on the right side, exposing part of the posterior root of M2. On the left side, a third vacuity is present exposing the posterior root of M1. In occlusal view, posterior to the roots of M3, the crown of M4 was in the process of erupting.

In the dentary, m4 is almost completely erupted. The dp3 is still in place with no evidence of p3. No dental wear is present.

Stage IIIb This stage is only represented by a dentary, with no associated cranial material. Compared to Stage IIIa, the dentary has increased in length, with the coronoid process departing the ramus posterior to m4. There is a longer diastema between c and p1, and between p1 and p2. There is a new diastema between p2 and dp3.

Stage IIIc This stage is also only represented by a dentary. The dp3 has been evulsed and p3 is erupting with the tip of its main cusp above the level of the alveolar platform. There is light wear on m1 only.

Stage IV Compared to the skull of Stage IIIa, the postorbital constriction is more posteriorly positioned, suggesting further frontal growth anteriorly. The posterior part of the skull seems unchanged. Anteriorly, the nasals and maxilla are longer. The antorbital fossa is deeper, and vacuities are present on both side exposing the roots of M2 and M3. The maxilla is completely formed posterior to the alveoli of M4, suggesting that this tooth was fully erupted. Two fully formed roots are also present for P3. Light wear is present on M1-2.

In the dentary, further elongation and thickening has occurred between Stage IIIc and IV. The distance between the mental foramina has increased. The p2 is further away from m1, giving plenty of room for a completely-erupted p3. The coronoid process is also more posteriorly positioned, well behind m4. The p1 and p2 are raised above the level of the ramus, with the upper parts of their roots visible. Light wear is present on p1-2, m1-3.

Stage V This stage is represented by a maxilla and dentary with wear intermediate between Stage VI and Stage IV. The diastema between C1 and P1 is longer than in Stage IV, but may be due sexual dimorphism rather than growth (Stage IV is represented by female specimens; Stage V is represented by male specimens). The premolars have fully erupted with the upper parts of their roots visible. Wear is present on all premolars. On M1, StD is more worn than it was in Stage IV. Other molars are not present.

The dentary is also longer and deeper but, as for the maxilla, this may be because of sexual dimorphism. Unlike in Stage IV, the p3 crown has erupted above the level of the alveolar platform and strongly reclines posteriorly. Wear is present on all teeth.

Stage VI This stage is represented by male specimens, which are larger in all dimensions than the corresponding dimensions in Stage IV's female specimens except in dental dimensions, which are not significantly larger. The antorbital fossa is deeper and the maxilla in this region is thicker, with the vacuities reduced to two tiny holes below M2 and M3. M1-4 are heavily worn, almost obliterating the stylar shelves of M1 and M2. In the dentary, p1 and p2 are also reclined. Tooth wear is heavy on all teeth, with increasing wear anteriorly compared to posteriorly. On the molars, the protoconid, paraconid, entoconid, and associated cristids are more worn than the metaconid, hypoconid, hypoconulid, and associated cristids.

Quantitative Analyses

Dental measurement plots are shown in Fig. 10 for the upper dentition and Fig. 11 for lower dentition. Considering *M. variae* from Riversleigh's Faunal Zone B, there are no obvious distinction between male and female specimens in terms of upper molar (Fig. 10) and lower premolar and molar size (Fig. 11) , both falling within the same range as the unknown sex specimen. This is not the case, however, for upper premolars (Fig. 10) where female specimens tend to have a longer and wider P1 and a wider but shorter P2 and P3 than male specimens. Specimens of *M. variae* from Riversleigh's Faunal Zone C are generally smaller in size, both in width and length for both upper and lower dentitions (Figs. 10, and 11) except for p3 whose size approximates that in Faunal Zone B specimens. Specimens of *M. encorensis* follow that trend in size, having smaller teeth than *M. variae*. The only specimen from Leaf Locality, Kutjamarpu LF, falls within the range of the Faunal Zone B specimens.

Univariate statistics for specimens of *M. variae* are shown in Appendix 5. Coefficients of variation (CVs) for *M. variae* range between 6.5 and 14.45, generally falling within the expected range (4–10) for a single mixed-sex population (Simpson et al. 1960). The m4 was the least variable tooth in length but it was also the most variable in posterior width (CVs 6.5-14.45). Other than the posterior width of m3, only the widths of p1, P2, and P3 had values that exceeded 10 (CVs 10.2-11.7).

Phylogenetic Analyses

Species of *Madju* are recovered within crown-group Peramelemorphia as the sister group to all Australian species (Peramelinae + Chaeropodidae + Thylacomyidae) in the

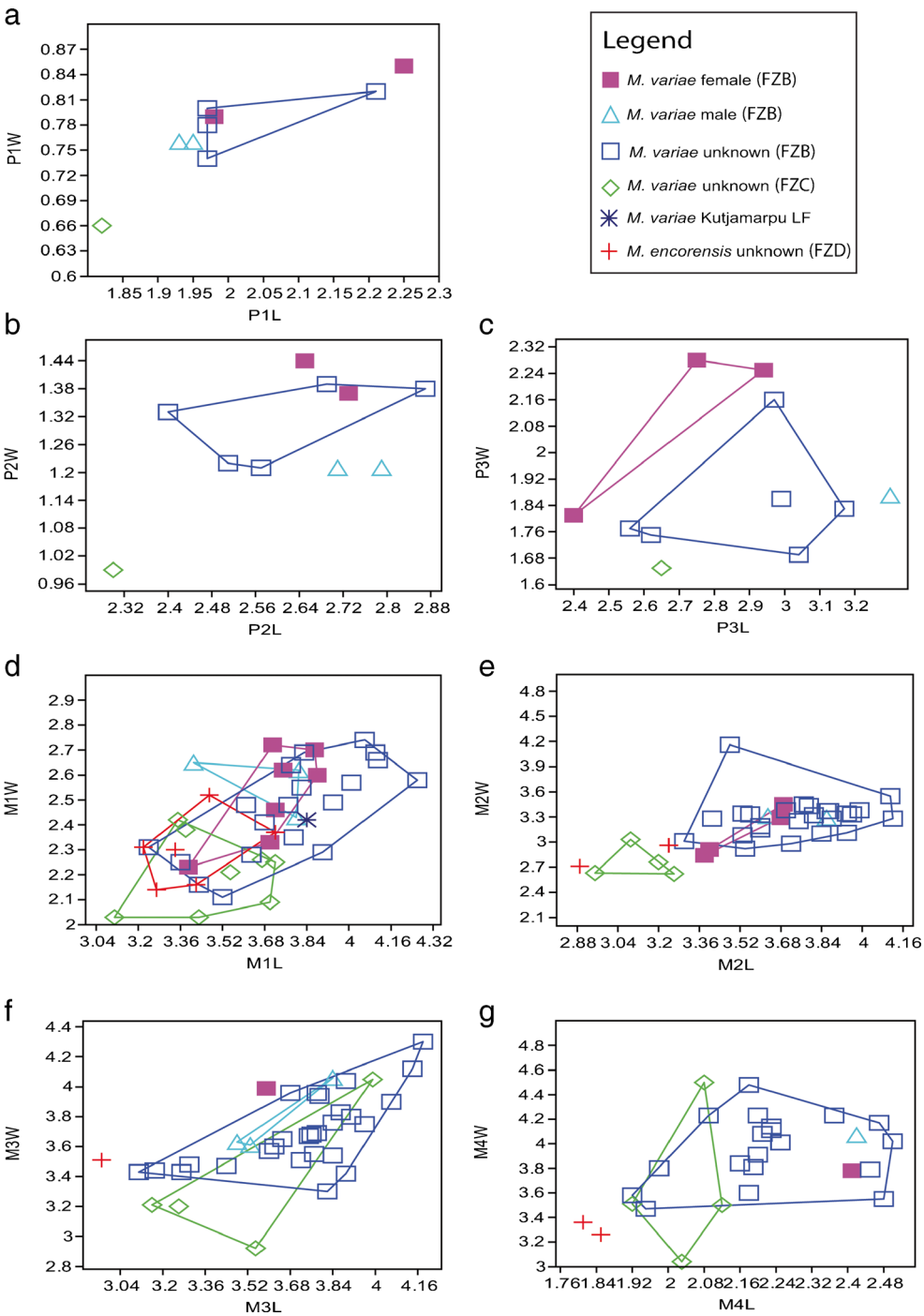

Fig. 10 XY plots of length versus width in millimeters of upper premolars and molars of species of *Madju,* gen. nov. **a**, P1; **b**, P2; **c**, P3; **d**, M1; **e**, M2; **f**, M3; **g**, M4. Convex hulls show the range of morphology of the group

maximum parsimony analysis (Fig. 12a), to the exclusion of peroryctines, but with weak support (bootstrap = <50 %; decay index = +1). In the maximum parsimony with a molecular scaffold (Fig. 12b) relationships are highly unresolved with species of *Madju* recovered in a clade containing all modern and fossil peramelemorphian to the exclusion of Yaralidae. A similar relationship is recovered in the Bayesian analysis with a molecular scaffold (Fig. 13b), except that Yaralidae is no longer excluded from the modern and fossil peramelemorphian clade. In the unconstrained Bayesian analysis, species of *Madju* are recovered as the sister group to the crown-group Peramelemorphia (Fig. 13a), but also with weak support (Bayesian posterior probability = 0.57). There is strong support, however, for the inclusion of both species within the same genus, recovered in all four analyses, with strong support values in both the parsimony (bootstrap =

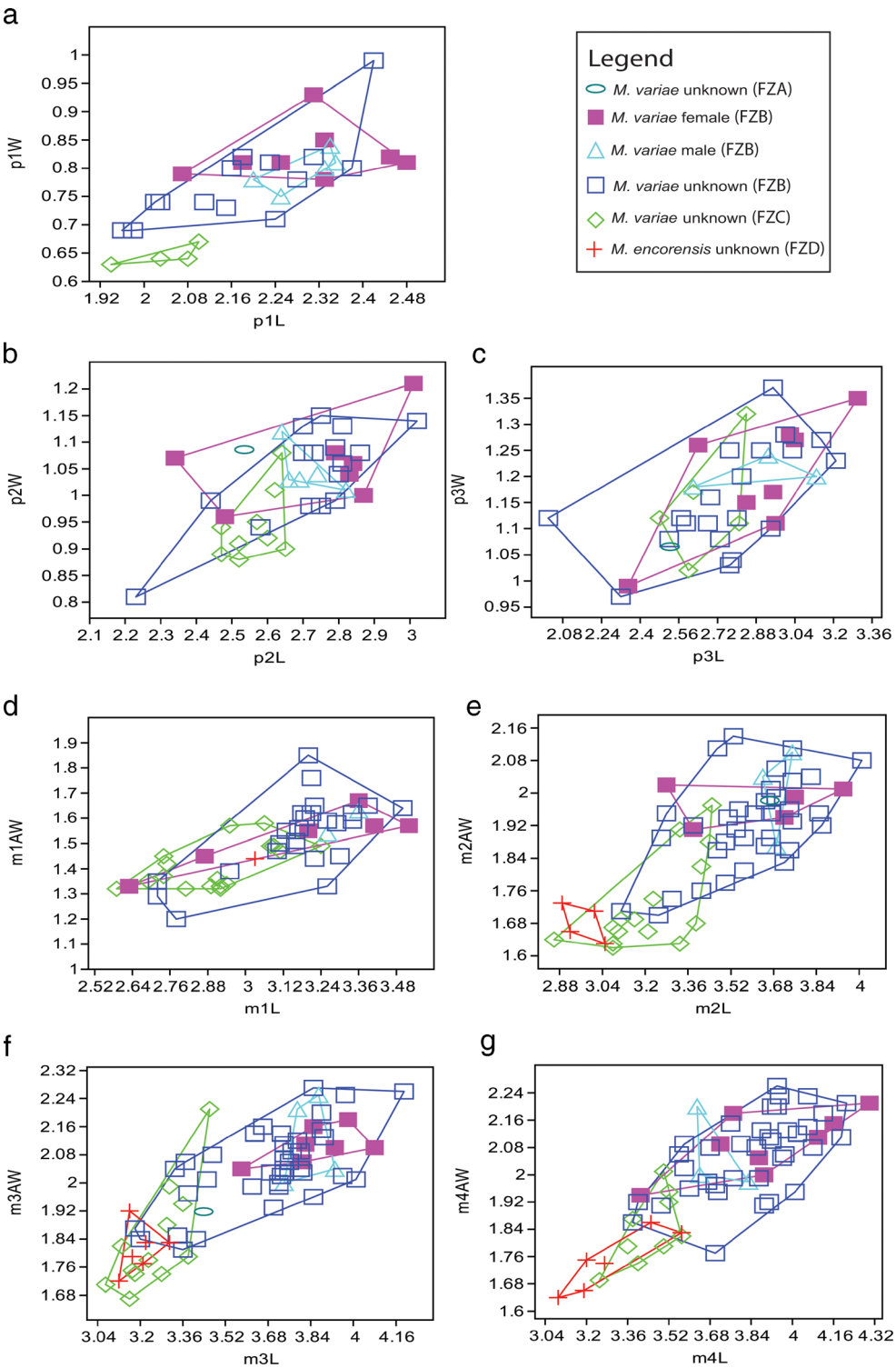

Fig. 11 XY plots of length versus width in millimeters of lower premolars and molars of species of *Madju,* gen. nov. **a**, p1; **b**, p2; **c**, p3; **d**, m1; **e**, m2; **f**, m3; **g**, m4. Convex hulls show the range of morphology of the group

72 %; decay index = +3) and Bayesian analyses (Bayesian posterior probability = 0.74).

Species of *Galadi, Bulungu,* and cf. *Perorctes* constantly fall outside of the crown-group (Figs. 12 and 13), with species of *Galadi* forming a well-supported clade (bootstrap = 58 %; decay index = +1; Bayesian posterior probability = 0.87). Peramelidae is not recovered in any analyses. Peroryctinae+ Echymiperinae is recovered in both the maximum parsimony (Fig. 12a) and unconstrained Bayesian analysis (Fig. 13a) as the sister group to a clade containing Peramelinae, Chaeropodidae, and Thylacomyidae, but this relationship is weakly supported (bootstrap = <50 %; decay index = +1;

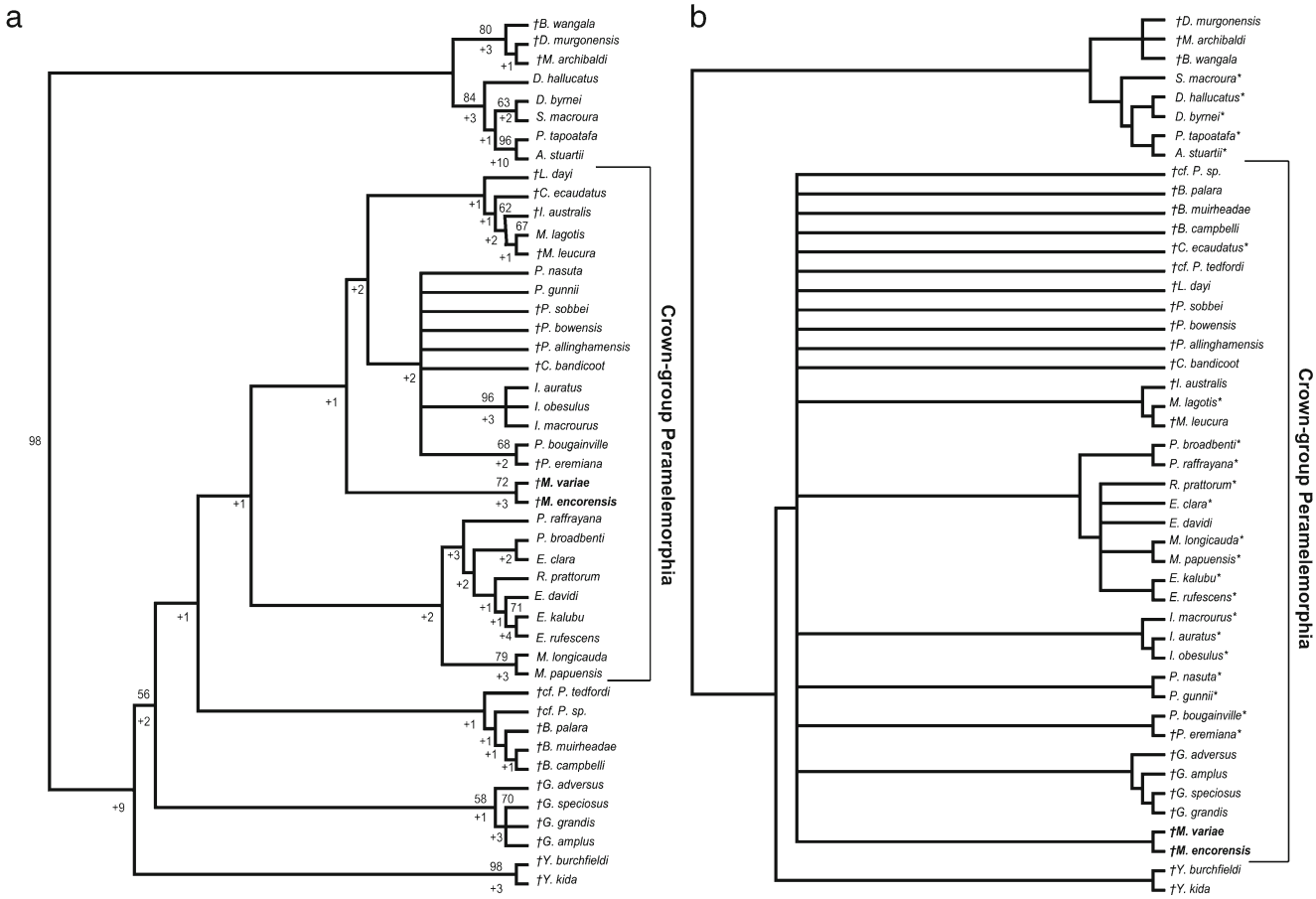

Fig. 12 Phylogenetic relationships of species of *Madju,* gen. nov., based on maximum parsimony analysis of a 156 character craniodental matrix. Fossil and recently extinct taxa are indicated by †. Crown-group Peramelemorphia is indicated. **a,** strict consensus of 12 most parsimonious trees (tree length = 873; consistency index excluding uninformative characters = 0.29; retention index = 0.6506) from unconstrained maximum parsimony analysis of the matrix; numbers above branches represent bootstrap values (1000 replicates); numbers below branches represent decay indices. **b,** strict consensus of 1743 most parsimonious trees (tree length = 902; consistency index excluding uninformative characters = 0.2806; retention index = 0.6342) that result when the matrix is analyzed using maximum parsimony and enforcing a 'backbone' molecular scaffold based on Westerman et al. (2012)

Bayesian posterior probability = 0.56). *Liyamayi dayi* and *Crash bandicoot* are recovered within the crown-group.

Discussion

Sexual Dimorphism in *Madju variae*

Madju variae was originally regarded in a PhD thesis (Muirhead 1994) to probably represent two species based on five specimens (including two skulls, two maxillae, and three dentaries, two of which were associated with one of the skulls). At that time, no specimens had been recovered from Encore Site, thus *M. encorensis* was unknown. The two taxa proposed by Muirhead (1994) were regarded to differ from each another in overall size, the condition of the centrocrista, and the development of the antorbital fossa. These two taxa were subsequently noted as 'Peramelemorphia new genus 4 sp. 1' and '2' in Archer et al. (2006), and Travouillon et al. (2006, 2009, 2011).

Sexual dimorphism is common among peramelemorphians (Gordon and Hulbert 1989; Strahan 1995; Aplin et al. 2010), with some of the most extreme cases occurring in larger species such as *Isoodon macrourus* (Lyne and Mort 1981), *Macrotis lagotis* (Johnson 1989), *Peroryctes broadbenti* (Aplin et al. 2010), and *Echymipera clara* (Flannery 1995), where males are much larger and more robust than females. They may even be twice the size of the females with larger and more elongate canines being conspicuously different features. However, until now no cases of sexual dimorphism have been reported from the fossil record. Here we suggest that the two taxa noted by Archer et al. (2006) and Travouillon et al. (2006, 2009, 2011) represent a single dimorphic species, for the following reasons.

1. Our analyses of the dental measurements of specimens of *Madju* show that coefficients of variation (CVs) for *M. variae* range between 6.5 and 14.45, generally falling

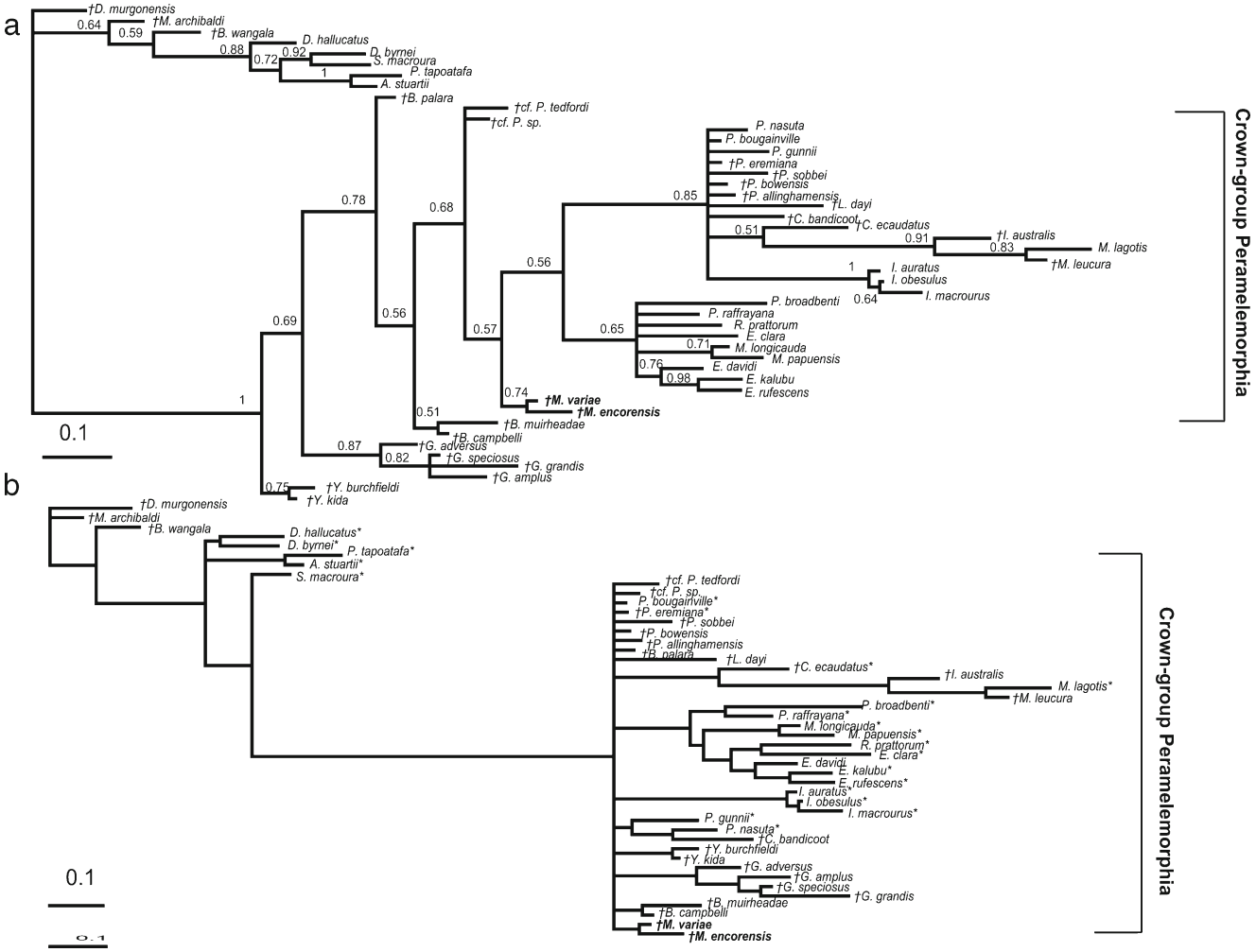

Fig. 13 Phylogenetic relationships of species of *Madju,* gen. nov., based on Bayesian analysis of a 156 character craniodental matrix. Fossil and recently extinct taxa are indicated by †. Crown-group Peramelemorphia is indicated. Numbers above branches represent Bayesian posterior probabilities. **a,** 50 % majority rule consensus that results after unconstrained Bayesian analysis of the matrix assuming the Mk + G model; the analysis was run for 20 million generations, sampling trees every 2000 generations. **b,** 50 % majority rule consensus that results after Bayesian analysis of the matrix assuming the Mk + G model and enforcing a 'backbone' molecular scaffold based on Westerman et al. (2012); the analysis was run as was the unconstrained Bayesian analysis. Branch lengths are proportional to the number of character state changes

within the expected range (4–10) for a single mixed-sex population (Simpson et al. 1960). The only CVs above 10 were for the posterior width of m4, and the width of the upper premolars. These CV values are consistent with those of modern bandicoots (Gurovich et al. 2013), which tend to be more variable in these measurements, especially in dimorphic peramelemorphians such as *Peroryctes broadbenti* (Aplin et al. 2010) and *Echymipera clara* (Flannery 1995), which show a huge difference in premolar size between males and females.

2. Travouillon (2008) calculated the estimated body mass of 'Peramelemorphia new genus 4 sp. 1' and '2'. 'Species 1' ranged in weight between 549 and 787 grams, while 'species 2' ranged between 890 and 1487 grams. The differences between these weight estimates are consistent with the differences in body mass for females and males of individual modern species (Gordon and Hulbert 1989; Strahan 1995; Aplin et al. 2010).

3. In dimorphic peramelemorphians, males tend to be larger in size and have larger and taller canines (Aplin et al. 2010). There are no examples of females having larger canines than males. Muirhead (1994)'s 'species 1' is smaller with small canines, while 'species 2' is large with large and tall canines. Specimens subsequently found from the same fossil deposits at Riversleigh show the same trend of small canines with small skulls/jaws and large canines with large skulls/jaws. This suggests that 'species 1' represents the females and 'species 2' the males of a single species.

4. Muirhead (1994) differentiated the two species of *Madju* by the condition of the centrocristae, which were incomplete (postparacrista and premetacrista do not join) in 'species 1' and complete in 'species 2.' However, it was noted that they

were not complete in all specimens of 'species 2.' Re-examination of the three specimens involved, QM F23406, F23429, and F23430, found that the least worn specimen (QM F23430) had incomplete centrocristae, while the other two were extremely worn and it was not clear where the postparacrista and premetacrista ended. Hence the complete centrocrista of 'species 2' is most likely a result of wear rather than a species-specific feature. Specimens found subsequent to this original assessment have supported the interpretation reported in the present study.

5. Antorbital fossa development is linked to size. In dimorphic peramelemorphians, males tend to have deeper antorbital fossae than females (pers. observ. K.J.T.). This difference interpreted previously to be an indication of specific difference, is therefore regarded here as a sexually dimorphic feature.

Phylogeny of Peramelemorphians

Our phylogenetic analyses support allocation of both new species of *Madju* within a single genus, but the relationships of these two species to other peramelemorphian are much less well resolved. Disregarding the two constrained analyses (Figs. 12b and 13b), which did not resolve their phylogenetic position, species of *Madju* are placed either within crown-group Peramelemorphia as sister to all Australian taxa in the maximum parsimony analysis, or sister to the whole of crown-group Peramelemorphia in the Bayesian analysis. However, neither position had strong support.

In all modern peramelemorphians the squamosal and frontal bones contact on the sidewall of the braincase (Muirhead 2000). This is considered to be the apomorphic (but frequently convergent) condition within Marsupialia. Until now, all extinct peramelemorphians represented by cranial material exhibit the plesiomorphic alisphenoid-parietal contact, such as *Yarala burchfieldi* (Muirhead 2000), *Galadi speciosus* (Travouillon et al. 2010), and *Bulungu palara* (Gurovich et al. 2013). *Madju variae* is the only fossil taxon known to have had a squamosal-frontal contact. The contact suture between these two bones, however, is shorter than that of modern species. This suggests that the condition for at least this species of *Madju* could be annectent between the archaic and modern groups of peramelemorphians.

The distribution of this character within Peramelemorphia, as well as other marsupial groups, indicates that it is a phylogenetically stable feature within groups and it is not known to have been convergently developed within this order (Muirhead 2000). If this is the case, squamosal/frontal contact would be a synapomorphy for all modern peramelemorphians and a feature that rationalizes the monophyly of a clade that includes *Madju* with these modern taxa to the exclusion of *Yarala, Galadi,* and *Bulungu.* It is noteworthy to mention that the interruption of the upper molar centrocrista used to be a defining character for peramelemorphians but a remnant of a connected centrocrista is present in *Peroryctes broadbenti* (Aplin et al. 2010) and variations in the connection of the centrocrista exist in various fossil taxa (e.g., Muirhead and Filan 1995; Gurovich et al. 2013; Travouillon et al. 2010, 2013a, 2013b).

Another feature that appears to be relatively stable is the posterior extension of the nasals. All modern peramelemorphians and species of *Madju* have the posterior ends of the nasals terminating anterior to the orbital fossa. This condition occurs in both short- and long-nosed species and therefore does not appear to have a direct relationship with overall snout length. This is a second feature that supports monophyly of modern peramelemorphians and species of *Madju*. Other fossil taxa known from skulls show the plesiomorphic state with the proximal ends of the nasals extending back past the anterior margin of the zygomatic arch and the orbital fossa. This is the case for *Yarala buchfieldi*, *Galadi speciosus, G. amplus* and *B. palara* (Muirhead 2000; Travouillon et al. 2010, 2013a; Gurovich et al. 2013).

A third feature that supports placement of *Madju* within or close to modern peramelemorphians is the condition of the primary and secondary foramen ovale. Species of *Madju* are the only fossil peramelemorphians that show the derived peramelemorphian condition of having both a primary and secondary foramen ovale. All other fossil species known from cranial remains retain a large primary foramen ovale. All modern peramelemorphians have some form of a secondary foramen ovale (with or without the concurrent presence of a primary foramen ovale). Species of *Madju*, however, are more derived in this feature than some modern New Guinean species in the greater separation of the secondary foramen ovale from the petrosal and the development of tunnelling around this foramen. In this difference, this feature places species of *Madju* closer to modern Australian than New Guinean taxa.

However, caution is appropriate with respect to conclusions about the relationships of *Madju* to other peramelemorphians considering some of the uncertainties in this study in revealing higher-level phylogenetic relationships noted above. For example, in the current analyses Peramelidae has not been recovered and Peroryctinae and Echymiperinae are presented as the sister group to Chaeropodidae, Thylacomyidae, and Peramelinae (Travouillon et al. 2010, 2013a, 2013b; Gurovich et al. 2013). This is despite the fact that molecular phylogenies indicate that Peramelidae is monophyletic (Meredith et al. 2008; Westerman et al. 2012). We suggest that until further evidence is available, species of *Madju* be treated as basal members of the Superfamily Perameloidea along with other fossil taxa (including *Galadi, Bulungu,* cf. *Peroryctes,* etc.) to the exclusion of species of *Yarala* (Superfamily Yaraloidea, Family Yaralidae).

Ontogeny of *Madju variae*

The tooth eruption stage seen in Stage I (dP3, M1, M2 + dp3, m1, m2, m3) is consistent with that of *Perameles nasuta* at 61 days old (Kingsmill 1962) and of *Isoodon macrourus* between 45–77 days (Lyne and Mort 1981). This is around the time (50–54 days) that juveniles leave the pouch in these two species (Gordon and Hulbert 1989). In contrast, the Greater Bilby, *Macrotis lagotis,* does not leave the pouch until it is 80 days old (McCraken 1990). Unfortunately, there are no tooth eruption studies for the latter species thereby prohibiting direct comparisons.

The tooth eruption of Stage II (dP3, M1, M2, M3 + dp3, m1, m2, m3, m4 erupting) is consistent with that of *Isoodon macrourus* between 80–94 days (Lyne and Mort 1981) and partially with that of *Perameles nasuta* at 126 days old (Kingsmill 1962) when m4 is fully erupted in this species. No dental wear is present on any of the teeth of *M. variae* at this stage, suggesting that it was not fully weaned at this time, subsisting on mother's milk instead of solid foods. In contrast, juveniles of both *Isoodon macrourus* and *Perameles nasuta* are fully weaned within 10 days of leaving the pouch, and start to have dental wear as a result of eating solid foods (Gordon and Hulbert 1989). In *Macrotis lagotis,* the young remain in the burrow for 14 days after leaving the pouch (around 94 days old) and are dependent on suckling from the mother (Johnson and Johnson 1983; McCraken 1990). Only after leaving the burrow do they start to eat solid foods and presumably begin to accumulate dental wear from food abrasion or from grit (bandicoot and bilbies dig out the majority of their food, eating grit attached to it, which contributes to dental wear). The juveniles continue to share the burrow with their mother for 160 days, possibly suckling during the day (Johnson and Johnson 1983; McCraken 1990).

It is also during Stage II that the sutures of the posterior part of the skull completely close or fuse while the remaining parts of the skulls continue to develop. This suggests that the neurocranium stops growing early on in the development of the juvenile and the remaining growth is principally related to snout and dental development. It is not possible to compare the timing of the closure of sutures with modern peramelemorphians because no comparable study exists. The only cranial ontogenetic study done on modern peramelemorphians compares only one juvenile stage to adults (Flores et al. 2013).

The tooth eruption stage seen in Stage IIIa (dP3, M1, M2, M3, M4 erupting + dp3, m1, m2, m3, m4 erupting) departs from both *Perameles nasuta* and *Isoodon macrourus.* In *P. nasuta,* when M4 starts to erupt at 137 days old (Kingsmill 1962), m4 is fully erupted and P3 and p3 become visible although dP3 and dp3 are still in place. In *I. macrourus,* M4 erupts after m4, P3 and p3 are fully erupted between 124–164 days (Lyne and Mort 1981). Here again, there is no dental wear on any teeth, at least until Stage IIIc, when p3 is erupting at which point m1 exhibits the first evidence of slight tooth wear.

The tooth eruption stage seen in Stage IV is that of an adult, with all teeth erupted. In *P. nasuta,* all teeth are fully erupted sometime between 137 and 361 days old (Kingsmill 1962) while in *I. macrourus,* all teeth are fully erupted by around 230 days (Lyne and Mort 1981).

Overall, it seems that *M. variae* does not develop as quickly as *P. nasuta* or *I. macrourus*, taking longer to erupt its upper and lower third premolars and much longer to be weaned. The growth and development of juvenile *M. variae* was probably much closer to that of *M. lagotis*. The phylogeny could suggest that the rapid growth and fast rate of reproduction of modern bandicoots, which is unique among marsupials, and comparable to rodents among placentals, may have evolved as a specialization after the separation of *Madju* from other crown-group peramelemorphians, probably sometime after the middle Miocene, and that thylacomyids retained the plesiomorphic state. However, we have not been able to compare this ontogenetic series with peramelid genera such as *Echymipera* or *Peroryctes* because no data have been published. It is possible that our interpretations may need revision once data for these taxa are available.

Biostratigraphy and palaeoenvironment of species of *Madju*

Madju variae has been recovered from one Faunal Zone A site (White Hunter LF), late Oligocene in age, 14 Faunal Zone B sites (Wayne's Wok, Inabeyance, Camel Sputum, Neville's Garden, Upper Site, Cadbury's Kingdom, Creaser's Ramparts, Dirk's Towers, Judith's Horizontalis, Mike's Menagerie, Price Is Right, Quantum Leap, RSO, and VIP LFs), early Miocene in age, and 11 Faunal Zone C sites (AL90, Gag, Golden Steph, Gotham City, Henk's Hollow, Jim's Carousel, Main Site, Rick's Sausage, Ringtail , Two Trees, and Wang LFs), middle Miocene in age, and one site PPFF Site, of unknown age (Archer et al. 1997; Arena 2004; Travouillon et al. 2006, 2011, 2013a). This species has a fairly long temporal range similar to taxa such as *Bulungu palara* (Gurovich et al. 2013), *Ekaltadeta ima* (Archer et al. 2006; Travouillon et al. 2011), but less so than *Burramys brutyi* (Brammall and Archer 1997). However, there are some differences between specimens of *M. variae* from Faunal Zone B and C, notably in the morphology of M1 (see description) and in the size of the specimens, which appear to be on average larger in Faunal Zone B than in Faunal Zone C (Figs. 10, and 11). Specimens of *M. encorensis* are also small, either equal in size to Faunal Zone C *M. variae* specimens, or smaller (Figs. 10, and 11). This may be reflecting an evolutionary trend within the genus such that species of *Madju* are reducing in size over time, possibly in response to regional environmental change during the Miocene from wet rainforest to more open forest environments (Archer et al. 1997; Travouillon et al. 2009). If this

did happen, then the oldest specimens should also be the largest. The largest specimens of *M. variae* are from White Hunter Site and Dirk's Towers Site. Although, dental measurements of specimens from White Hunter Site and Dirk's Towers Site are within the range of other Faunal Zone B specimens and morphologically identical, the dentaries QM F57561 and QM F20890 are the most robust and longest specimens (respectively) so far discovered at Riversleigh, and the partial skull QM F39857 (mostly crushed) has the longest maxilla, longest zygomatic arch and deepest antorbital fossa. Dirk's Towers Site may be one of the oldest within Faunal Zone B, containing the most plesiomorphic species of *Galadi* (*G. adversus,* Travouillon et al. 2013a) and *Yarala* (*Y. kida,* QM F36340).

Madju variae was also recovered from the Kutjamarpu LF of the Wipajiri Formation in the Tirari Desert of South Australia. It is the second species of peramelemorphian shared between the Riversleigh World Heritage Area deposits and those of the mid Cenozoic sediments of South Australia, the first being *Bulungu palara* (Gurovich et al. 2013). The age of the Kutjamarpu LF has been long debated (Woodburne et al. 1993; Archer et al. 1994, 1995; Travouillon et al. 2006; Megirian et al. 2010), but there is increasing support for an early Miocene age. For example, molar dimensions of *Neohelos tirarensis* from the Kutjamarpu LF consistently group with those of *N. tirarensis* from Riversleigh's FZB (Black et al. 2013a). In addition, a number of other Faunal Zone B taxa also occur in the Kutjamarpu LF including the casuariid *Emuarius gidju,* the phascolarctid *Litokoala kutjamarpensis*, the vombatid *Rhizophascolonus crowcrofti,* the thylacoleonid *Wakaleo oldfieldi,* the ektopodontid *Ektopodon serratus,* the pseudocheirid possums *Paljara tirarensae, Marlu kutjamarpensis, M. ampelos,* and *M. syke,* and the potoroid *Wakiewakie lawsoni* (Godthelp et al. 1989; Archer et al. 2006; Gillespie 2007; Louys et al. 2007; Roberts et al. 2008, 2009; Travouillon et al. 2011; Black et al. 2013b). Specimens of *M. variae* from the Kutjamarpu LF are closer in size to those from Riversleigh's FZB, supporting an early Miocene in age for this central Australian assemblage.

Conclusions

Two new species of peramelemorphians are described and named here. The first species, *Madju variae,* occurs in the Kutjamarpu Local Fauna from the Leaf Locality in the Wipajiri Formation of South Australia and late Oligocene to middle Miocene local faunas from the Riversleigh World Heritage Area. The second species, *Madju encorensis*, occurs in the late middle to early late Miocene Encore Local Fauna of the Riversleigh WHA. Our phylogenetic analyses suggest that these species form a clade that is the sister-group to crown-group Peramelemorphia. We suggest that they represent basal members of Perameloidea, one of the two Superfamilies within Peramelemorphia (the other being Yaraloidea), as do species of *Galadi, Bulungu,* and cf. *Peroryctes*. Species of *Madju* appear to show reduction in size through time, possibly as a result of environmental change during the Miocene. *Madju variae* shows evidence of sexual dimorphism consistent with modern bandicoot taxa. This is the first record of a sexually dimorphic peramelemorphian in the fossil record. *Madju variae* is also represented by the first ontogenetic series for a fossil peramelemorphian. The results of the assessment of ontogenetic change suggest that growth and development of *M. variae* juveniles was much slower than that of modern peramelines (e.g., species of *Isoodon* and *Perameles*), with the third upper and lower premolars erupting at a later stage. The same appears to be true with respect to dental wear, which manifests itself at a relatively late developmental stage suggesting that weaning occurred much later than it does in modern peramelids but possibly at a time more comparable to that seen in the thylacomyid *Macrotis lagotis*. The rapid developmental pace of modern bandicoots is therefore thought to be a specialisation that evolved secondarily.

Acknowledgments Support for research at Riversleigh has come from the Australian Research Council (LP0989969, LP100200486, DP1094569 & DP130100197 grants to M. Archer and S.J. Hand at the University of New South Wales); XSTRATA Community Partnership Program (North Queensland); the University of New South Wales; P. Creaser and the CREATE Fund; the Queensland Parks and Wildlife Service; Environment Australia; the Queensland Museum; the Riversleigh Society Inc.; Outback at Isa; Mount Isa City Council; private supporters including K. & M. Pettit, E. Clark, M. Beavis, and M. Dickson; and the Waanyi people of northwestern Queensland. Assistance in the field has come from many hundreds of volunteers as well as staff and postgraduate students of the University of New South Wales. We thank R. Day for providing funding to the University of Queensland to create a postdoctoral position for K. J. Travouillon. We thank S. Ingleby and A. Divljan from the Australian Museum, H. Janetzki from the Queensland Museum, and C. Stevenson from the Western Australian Museum for providing access to modern bandicoot specimens. We thank the UNSW Palaeosciences Lab and the UQ Palaeo Hub for their support and anonymous reviewers for helpful comments.

References

Aplin KP, Archer M (1987) Recent advances in marsupial systematics with a new syncretic classification. In: Archer M (ed) Possums and Opossums: Studies in Evolution, Volume 1. Surrey Beatty & Sons, Sydney, pp xv-lxxii

Aplin KP, Helgen KM, Lunde DP (2010) A review of *Peroryctes broadbenti*, the giant bandicoot of Papua New Guinea. Am Mus Novitates 3696:1–41

Archer M (1976) The dasyurid dentition and its relationships to that of didelphids, thylacinids and borhyaenids. Australian J Zool, Suppl Ser 39:1–34

Archer M, Arena DA, Bassarova M, Beck RMD, Black K, Boles WE, Brewer P, Cooke BN, Crosby K, Gillespie A, Godthelp H, Hand SJ,

Kear BJ, Louys J, Morrell A, Muirhead J, Roberts KK, Scanlon JD, Travouillon KJ, Wroe S (2006) Current status of species-level representation in faunas from selected fossil localities in the Riversleigh World Heritage Area, northwestern Queensland. Alcheringa Spec Iss 1:1–17

Archer M, Hand SJ, Godhelp H (1994) Patterns in the history of Australia's mammals and inferences about palaeohabitats. In: Hill R (ed) History of the Australian Vegetation. Cambridge University Press, Cambridge, pp 80–103

Archer M, Hand SJ, Godhelp H (1995) Tertiary environmental and biotic change in Australia. In: Vrba ES, Denton GH, Partridge TC, Burckle LH (ed) Paleoclimate and Evolution, with Emphasis on Human Origins. Yale University Press, New Haven, pp 77–90

Archer M, Hand SJ, Godthelp H, Creaser P (1997) Correlation of the Cainozoic sediments of the Riversleigh World Heritage fossil property, Queensland, Australia. In: Aguilar J-P, Legendre S, Michaux J (ed) Actes du congrès BiochroM'97, Mémoires et Travaux de l'Ecole Pratique des Hautes Etudes,Institut de Montpellier 21:131–152

Arena DA (2004) The geological history and development of the terrain at the Riversleigh World Heritage Area during the middle Tertiary. Ph.D. Dissertation, University of New South Wales, Sydney

Beck RMD (2008) A dated phylogeny of marsupials using a molecular supermatrix and multiple fossil constraints. J Mammal 89(1):175–189

Beck RMD, Godhelp H, Weisbecker V, Archer M, Hand SJ (2008) Australia's oldest marsupial fossils and their biogeographical implications. PloS ONE 3(3):e1858

Black KH, Archer M, Hand SJ, Godthelp H (2010) First comprehensive analysis of cranial ontogeny in a fossil marsupial—from a 15-million-year-old cave deposit in northern Australia. J Vertebr Paleontol 30(4):993–1011

Black KH, Archer M, Hand SJ, Godthelp H (2013a) Revision in the diprotodontid marsupial genus *Neohelos*: systematics and biostratigraphy. Acta Palaeontol Polonica 58(4):679–706

Black KH, Louys J, Price GJ (2013b) Understanding morphological variation in the extant koala as a framework for identification of species boundaries in extinct koalas (Phascolarctidae; Marsupialia). J Syst Palaeontol doi:DOI:10.1080/14772019.2013.768304

Brammall J, Archer M (1997) A new Oligocene-Miocene species of *Burramys* (Marsupialia. Burramyidae) from Riversleigh. northwestern Queensland. Mem Queensland Mus 41(2):247–268

Flannery T (1995) Mammals of New Guinea. Reed Books, Australia

Flores DA, Abdala F, Giannini NP (2013) Post-weaning cranial ontogeny in two bandicoots (Mammalia, Peramelemorphia, Peramelidae) and comparison with carnivorous marsupials. J Zool 116:372–384 doi: http://dx.doi.org/10.1016/j.zool.2013.07.003

Gillespie AK (2007) Diversity and systematics of marsupial lions from the Riversleigh World Heritage Area and the evolution of the Thylacoleonidae. Ph.D. Dissertation, University of New South Wales, Sydney

Godthelp H, Archer M, Hand SJ, Plane MD (1989) New potoroine from Tertiary Kangaroo Well Local Fauna, N.T. and description of upper dentition of potoroine *Wakiewakie lawsoni* from Upper Site Local Fauna, Riversleigh. In: 5th Conference on Australian Vertebrate Evolution, Palaeontology and Systematics, Abstracts, Sydney. University of New South Wales, p 6

Gordon G, Hulbert AJ (1989) Peramelidae. In: Walton DW (ed) Fauna of Australia vol Vol. 1B: Mammalia. Australian Government Publishing Service, Canberra, pp 603–624

Gurovich Y, Travouillon KJ, Beck RMD, Muirhead J, Archer M (2013) Biogeographical implications of a new mouse-sized fossil bandicoot (Marsupialia: Peramelemorphia) occupying a dasyurid-like ecological niche across Australia. J Syst Palaeontol doi:10.1080/14772019.2013.776646

Johnson C, Johnson KA (1983) Behaviour of the Bilby, *Macrotis lagotis* (Reid) in captivity. Australian Wildl Res 10:77–87

Johnson KA (1989) Thylacomyidae. In: Walton DWE (ed) Fauna of Australia. Australian Government Publishing Service, Canberra, pp 625–635

Kingsmill E (1962) An investigation of criteria for estimating age in the marsupials *Trichosurus vulpecula* Kerr and *Perameles nasuta* Geoffroy. Australian J Zool 10:597–616

Lewis PO (2001) A likelihood approach to inferring phylogeny from discrete morphological characters. Syst Biol 50:913–925

Louys J, Black K, Archer M, Hand SJ, Godhelp H (2007) Descriptions of koala fossils from the Miocene of Riversleigh, northwestern Queensland and implications for *Litokoala* (Marsupialia, Phascolarctidae). Alcheringa 31:99–110

Luckett WP (1993) An ontogenetic assessment of dental homologies in therian mammals. In: Szalay FS, Novacek MJ, McKenna MC (eds) Mammal Phylogeny: Mesozoic Differentiation, Multituberculates, Monotremes, Early Eutherians and Marsupials. Springer-Verlag, New York, pp 182–204

Lyne AG, Mort PA (1981) A comparison of skull morphology in the marsupial bandicoot genus *Isoodon*: its taxonomic implications and notes on a new species, *Isoodon arnhemensis*. Australian Mammal 4:107–133

McCraken HE (1990) Reproduction in the Greater Bilby, *Macrotis lagotis* (Reid) - a comparison with other perameloids. In: Seebeck JH, Brown PR, Wallis RL, Kemper CM (eds) Bandicoots and Bilbies. Surrey Beatty & Sons, Sydney, pp 199–204

Megirian D, Prideaux GJ, Murray PF, Smit N (2010) An Australian land mammal age biochronological scheme. Paleobiology 36:658–671

Meredith RW, Westerman M, Springer MS (2008) A timescale and phylogeny for "bandicoots" (Peramelemorphia: Marsupialia) based on sequences for five nuclear genes. Mol Phylogen Evol 47:1–20

Muirhead J (1994) Systematics, evolution and palaeobiology of recent and fossil bandicoots (Peramelemorphia, Marsupialia). Ph.D. Dissertation, University of New South Wales, Sydney

Muirhead J (2000) Yaraloidea (Marsupialia, Peramelemorphia), a new superfamily of marsupial and a description and analysis of the cranium of the Miocene *Yarala burchfieldi*. J Paleontol 74(3):512–523

Muirhead J, Filan SL (1995) *Yarala burchfieldi*, a plesiomorphic bandicoot (Marsupialia, Peramelemorphia) from Oligo-Miocene deposits of Riversleigh, northwestern Queensland. J Paleontol 69(1):127–134

Roberts KK, Archer M, Hand SJ, Godhelp H (2009) New Australian Oligocene to Miocene ringtail possums (Pseudocheiridae) and revision of the genus *Marlu*. Palaeontology 52(2):441–456

Roberts KK, Bassarova M, Archer M (2008) Oligo-Miocene ringtail possums of the genus *Paljara* (Pseudocheiridae: Marsupialia) from Queensland, Australia. Geobios 41:833–844

Simpson G, Roe A, Lewontin R (1960) Quantitative Zoology. Harcourt Brace, New York.

Sorenson MD, Franzosa EA (2007) Treerot ver. 3.0. Department of Biology BU, Boston, MA

Strahan R (1995) The Mammals of Australia. Reed New Holland, Sydney

Swofford DL (2002) PAUP*. Phylogenetic Analysis Using Parsimony (*and Other Methods). Version 4 (updated to 10 beta). Sinauer Associates, Sunderland, Massachussets

Travouillon KJ (2008) Palaeoecological and biochronological studies of Riversleigh, World Heritage Property, Oligo-Miocene Fossil Localities, North-Western Queensland, Australia. Ph.D. Dissertation, University of New South Wales, Sydney

Travouillon KJ, Beck RMD, Hand SJ, Archer M (2013b) The oldest fossil record of bandicoots (Marsupialia; Peramelemorphia) from the late Oligocene of Australia. Palaeontol Electron 16(2):13A 52p

Travouillon KJ, Archer M, Hand SJ, Godthelp H (2006) Multivariate analyses of Cenozoic mammalian faunas from Riversleigh, northwestern Queensland. Alcheringa Spec Iss 1:323–349

Travouillon KJ, Gurovich Y, Archer M, Hand SJ, Muirhead J (2013a) The genus *Galadi*: three new bandicoots (Marsupialia, Peramelemorphia) from Riversleigh's Miocene deposits, northwestern Queensland, Australia. J Vertebr Paleontol 33(1):153–168

Travouillon KJ, Escarguel G, Legendre S, Archer M, Hand SJ (2011) The use of MSR (Minimum Sample Richness) for sample assemblage comparisons. Paleobiology 37(4):696–709

Travouillon KJ, Gurovich Y, Beck RMD, Muirhead J (2010) An exceptionally well-preserved short-snouted bandicoot (Marsupialia; Peramelemorphia) from Riversleigh's Oligo-Miocene deposits, Northwestern Queensland, Australia. J Vertebr Paleontol 30(5):1528–1546

Travouillon KJ, Legendre L, Archer M, Hand S (2009) Palaeoecological analyses of Riversleigh's Oligo-Miocene sites: implications for Oligo-Miocene climate change in Australia. Palaeogeogr, Palaeoclimatol, Palaeoecol 276(1–4):24–37

Turnbull WD, Lundelius EL Jr, Archer M (2003) Dasyurids, perameloids, phalangeroids, and vombatoids from the early Pliocene Hamilton fauna, Victoria, Australia. Bull Am Mus Nat Hist 279:513–540

Voss RS, Jansa SA (2003) Phylogenetic studies on didelphid marsupials II. Nonmolecular data and new IRBP sequences: separate and combined analyses of didelphine relationships with denser taxon sampling. Bull Am Mus Nat Hist 276:1–82

Westerman M, Kear BP, Aplin K, Meredith RW, Emerling C, Springer MS (2012) Phylogenetic relationships of living and recently extinct bandicoots based on nuclear and mitochondrial DNA sequences. Mol Phylogen Evol 62:97–108 doi:10.1016/j.ympev.2011.09.009

Westerman M, Krajewski C (2000) Molecular relationships of the Australian bandicoot genera *Isoodon* and *Perameles* (Marsupialia: Peramelina). Australian Mammal 22:1–8

Westerman M, Springer MS, Dixon J, Krajewski C (1999) Molecular relationships of the extinct pig-footed bandicoot *Chaeropus ecaudatus* (Marsupialia: Perameloidea) using 12S rRNA sequences. J Mammal Evol 6:271–288

Westerman M, Springer MS, Krajewski C (2001) Molecular relationships of the New Guinean bandicoot genera *Microperoryctes* and *Echymipera* (Marsupialia: Peramelina). J Mammal Evol 8:93–105

Wible JR (2003) On the cranial osteology of the short-tailed opposum *Monodelphis brevicaudata* (Didelphidae, Marsupialia). Ann Carnegie Mus 72(3):137–202

Woodburne MO, MacFadden BJ, Case JA, Springer MS, Pledge N, Power JD, Woodburne J, Springer KB (1993) Land mammal biostratigraphy and magnetostratigraphy of the Etadunna Formation (late Oligocene) of South Australia. J Vertebr Paleontol 13:483–515

Worthy TH, Tennyson AJD, Archer M, Musser AM, Hand SJ (2006) Miocene mammal reveals a Mesozoic ghost lineage on insular New Zealand, southwest Pacific. Proc Natl Acad Sci USA 103:19419–19423